Emplacement temperatures of pyroclastic and volcaniclastic deposits in kimberlite pipes in southern Africa

G. Fontana[1], C. Mac Niocaill[1], R.J. Brown[2], R.S.J. Sparks[3], and M. Field[4]

[1]Department of Earth Sciences, University of Oxford, Parks Road, Oxford OX1 3PR, UK

[2]Department of Earth and Environmental Sciences, The Open University, Walton Hall, Milton Keynes MK7 6AA, UK

[3]Department of Earth Sciences, Wills Memorial Building, University of Bristol, Queen's Road, Bristol BS7 1RJ, UK

[4]DiaKim Consulting Limited, Wells Road, Wookey Hole, Wells, BA5 1DN, UK

Corresponding author: giovanni.fontana@earth.ox.ac.uk

Palaeomagnetic techniques for estimating the emplacement temperatures of volcanic deposits have been applied to pyroclastic and volcaniclastic deposits in kimberlite pipes in southern Africa. Lithic clasts were sampled from a variety of lithofacies from three pipes for which the internal geology is well constrained (the Cretaceous A/K1 pipe, Orapa Mine, Botswana, and the Cambrian K1 and K2 pipes, Venetia Mine, South Africa). The sampled deposits included massive and layered vent-filling breccias with varying abundances of lithic inclusions, layered crater-filling pyroclastic deposits, talus breccias and volcaniclastic breccias. Basalt lithic clasts in the layered and massive vent-filling pyroclastic deposits in the A/K1 pipe at Orapa were emplaced at >570°C, at 200–440°C in the pyroclastic crater-filling deposits, and at <180°C in crater-filling talus breccias and volcaniclastic breccias.

The results from K1 and K2 pipes at Venetia are suggestive of emplacement temperature estimates for the vent-filling breccias of 260°C to >560°C, although interpretation of these results is hampered by the presence of Mesozoic magnetic overprints. These temperatures are comparable to the estimated emplacement temperatures of other kimberlite deposits and fall within the proposed stability field for common interstitial matrix mineral assemblages within vent-filling volcaniclastic kimberlites. The temperatures are also comparable to those obtained for pyroclastic deposits in other silicic volcanic systems. Because the lithic content of the studied deposits is 10–30%, the initial bulk temperature of the pyroclastic mixture of cold lithic clasts and juvenile kimberlite magma could have been 300–400°C hotter than the palaeomagnetic estimates. Together with the discovery of welding and agglutination of juvenile pyroclasts in some pyroclastic kimberlites, the palaeomagnetic results indicate that there are examples of kimberlites where phreatomagmatism did not play a major role in the generation of the pyroclastic deposits. This study indicates that palaeomagnetic methods can successfully distinguish differences in the emplacement temperatures of different kimberlite facies.

Keywords: Kimberlite, Emplacement temperature, Palaeomagnetism, Pyroclastic deposits, Thermoremanent magnetization, Explosive eruption

Introduction

Kimberlites are mantle-derived ultramafic volcanic rocks preserved in dykes, volcanic pipes and craters (Dawson, 1971; Mitchell, 1986). Over 5000 kimberlite occurrences are known (Kjarsgaard, 1996), but are confined to the ancient cratonic regions of continents (e.g., south, central and western Africa; Canada, Australia, Russia). Their emplacement ages vary from early Proterozoic through to early Tertiary and because no kimberlite eruptions have ever been witnessed many aspects of kimberlite volcanism are unclear (Sparks et al, 2006). In addition, kimberlite rocks are usually highly altered, particularly the matrix – though less so for incorporated lithic clasts, and contaminated with mantle and crustal debris (Mitchell, 1986; Sparks et al., 2006; Stripp et al., 2006; Buse et al., 2010). This has made it difficult to reconstruct the fundamental properties of the magma, such as its chemistry, temperature, viscosity and volatile content (e.g., Sparks et al., 2006).

Two principal theories have been put forward as the driving force for kimberlite eruptions: (1) the exsolution of magmatic volatiles (e.g., Dawson, 1971; Clement and Reid, 1989; Field and Scott Smith, 1999; Sparks et al., 2006; Wilson and Head, 2007), and (2) the interaction of rising kimberlite magma with ground water (e.g., maar-diatreme model of Lorenz, 1975; Kurszlaukis et al., 1998; Lorenz and Kurszlaukis, 2007). Recent dynamical models propose a volatile-driven eruption mechanism similar to other types of explosive volcanic eruptions (see Sparks et al., 2006), and the similarities between steep-sided kimberlite pipes and maars and diatremes, formed during hydrovolcanic explosions, are striking. As in other varieties of volcanism the two models are not mutually exclusive.

The ability to estimate the emplacement temperatures of pyroclastic deposits using palaeomagnetic methods has proved useful in distinguishing between magmatic and phreatomagmatic modes of eruption, and in discriminating between pyroclastic deposits and epiclastic deposits (Aramaki and Akimoto, 1957; Wright, 1978; Hoblitt and Kellogg, 1979; Downey and Tarling, 1991; Bardot et al., 1996). The technique, pioneered by Aramaki and Arimoto (1957), has been successfully applied to many deposits around the world (Kent et al., 1981; Hoblitt and Kellogg, 1979; Clement et al., 1993; Mandeville et al., 1994; De'Gennaro et al., 1996; Cioni et al., 2004; McClelland et al., 2004; Porreca et al., 2008; Paterson et al., 2010). Palaeomagnetic emplacement temperature determinations of pyroclastic deposits have also been shown, in certain cases, to be as accurate as direct measurements taken shortly after eruption (e.g., the 1980 eruption of Mt. St. Helens; Paterson et al., 2010).

Several attempts have been made to estimate the emplacement temperatures of kimberlite deposits. The general absence of thermal metamorphic effects on entrained xenoliths and in adjacent country rocks has led some authors to propose emplacement temperatures of <500°C for volcaniclastic kimberlite deposits (e.g., Watson, 1967; Mitchell, 1986; Skinner and Marsh, 2004). Sosman (1938) deduced intrusion temperatures of 340°C for North American kimberlites from thermal effects on coal inclusions (see Watson, 1967). Stasiuk et al. (1999) used reflectance values in dispersed organic matter inclusions within Canadian kimberlites to deduce temperatures of 150–200°C for pipe-facies and <100°C for crater-facies volcaniclastic kimberlites. Palaeomagnetic studies by McFadden (1977) on wall

rock samples and accidental inclusions close to the contacts of four South African pipes suggested emplacement temperatures of ~300°C. The stability fields of the common alteration assemblages in kimberlite pyroclastic rocks give minimum temperatures of 250–400°C (Stripp et al., 2006; Buse et al., 2010).

Here we present the results of palaeomagnetic measurements of the emplacement temperatures of a range of pyroclastic and volcaniclastic kimberlite deposits within three contrasting kimberlite pipes in southern Africa, for which the internal geology is well constrained by recent geological studies (Field et al., 1997; Brown et al., 2009; Gernon et al., 2009a). Measurements of the thermoremanent magnetization (TRM) of included lithic clasts show that the range of emplacement temperatures varies from around ambient for volcaniclastic deposits, interpreted as talus breccias and debris flow deposits, through to >200 to >570°C for pyroclastic deposits – temperatures which are similar to those obtained for pyroclastic deposits in other volcanic systems. We discuss the implications of these results in the context of the supporting geological evidence for the mode of formation of the kimberlite deposits and for the nature of kimberlite eruptions.

Geological setting

Orapa A/K1 kimberlite pipe, Botswana

The Orapa A/K1 kimberlite (Fig. 1a and 2a) comprises two steep-sided coalescing pipes (north and south) that were intruded at ~92.1 Ma through Archaean basement (granite-

gneisses and tonalites) and Phanerozoic sediments and basalt lavas of the Karoo Supergroup (Field and Scott-Smith, 1999). The geology of the Orapa A/K1 pipe is described by Field et al. (1997) and Gernon et al. (2009a). The upper portions are dominated by a layered pyroclastic kimberlite lithofacies (Northern Pyroclastic Kimberlite, NPK; Fig. 1a) which is characterised by abundant basement and basalt fragments (≤10 m diameter). These fragments can be concentrated in crude, reverse- to normally graded layers. The matrix comprises abundant serpentinised olivine macrocrysts and phenocrysts and juvenile lapilli. Interstitial pore-space is filled with serpentine-diopside cement. At depth the layering disappears and the deposit becomes massive (Field et al., 1997).

The south pipe is larger than the north pipe and its crater cuts the north pipe (Field et al., 1997). Talus deposits outcrop along the western margin of the south pipe and comprise crudely bedded clast-supported basalt breccias and bedded crystal-rich grain flow deposits (Fig. 1a and 2a), both of which dip towards the centre of the pipe at the angle of repose (Field et al., 1997). Field et al. (1997) propose that these deposits formed by the post-eruption decrepitation of the pipe walls and a surrounding tephra cone. Inner crater lithofacies (Southern Volcaniclastic Kimberlite, SVK; Fig. 1a and 2a) comprise a sub-horizontally layered sequence of poorly sorted basalt-bearing lapilli-tuffs and breccias and stratified olivine tuffs and grits. These are interpreted as a series of ignimbrites derived from neighbouring pipes and sheet-flood deposits (Gernon et al., 2009a).

K2 and K1 pipe, Venetia Mine, South Africa

The Venetia kimberlite cluster is located in the Limpopo region of South Africa (Fig. 1b). It comprises 14 pipes outcropping over ~4 km^2 (Seggie et al., 1998; Kurszlaukis and Barnett, 2003). The pipes were intruded at ~519 Ma into complex Proterozoic basement comprising biotite gneiss, biotite schists and amphibolite gneiss, quartzo-feldspathic gneiss and metasediments (Phillips et al., 1999). Shale and lava clasts within the pipes indicate that Waterberg Formation rocks covered the basement at time of emplacement (Kurszlaukis and Barnett, 2003).

K2 is a steep-sided volcanic pipe which tapers at depth (Kurszlaukis and Barnett, 2003; Brown et al., 2009). It is 250 m by 300 m wide and is broadly divisible into two parts (Fig. 1b and 2b). K2 East is dominated by massive volcaniclastic kimberlite (MVK). K2 West is filled with crudely bedded coarse-grained country rock breccias (Br) and matrix- or clast-supported volcaniclastic kimberlite breccias (mVKBr, cVKBr) with variable amounts of lithic lapilli, blocks and boulders. The contact between these two halves is marked by a shear surface dipping ~64° westwards (Fig. 1b and 2b). The breccias in K2 are thought to result from two competing processes: (1) gravitational collapse of pipe margins that generated abundant brecciated country rock (Br lithofacies) and (2) proximal fallout of country rock clasts and pyroclasts from eruption jets during explosive eruptions (VKBr lithofacies; Brown et al., 2009). The breccias pre-date the MVK in K2 East, which represents the deposits of a later stage of explosivity in the pipe (Kurszlaukis and Barnett, 2003; Brown et al., 2009). K1 is an irregular-shaped kimberlite pipe that is mainly filled with MVK similar to that found in K2 (Fig. 1c and 2c; Kurszlaukis and Barnett, 2003; Walters et al., 2006).

Palaeomagnetic determination of emplacement temperatures

Palaeomagnetic determination of the emplacement temperatures of volcanic deposits relies on the fact that lithic clasts incorporated into a pyroclastic (or volcaniclastic) deposit will have originally been magnetized *in situ* prior to eruption and will thus possess a natural remanent magnetization (NRM) aligned with the Earth's magnetic field during their formation or during some metamorphic event. The nature of this pre-eruption magnetization is not critical to the interpretation. During the eruption these clasts are thrown into the air and 'jumbled up' such that the direction of magnetization will now vary from clast to clast when they come to rest. If the deposits are emplaced above ambient temperatures, the lithic clasts are heated during their incorporation into the deposit and will cool to ambient temperature in their present position. If the clast contains a population of magnetic grains with a spectrum of grain sizes, a portion of the original magnetization with unblocking temperatures (T_{ub}) less than or equal to the emplacement temperature (T_e) will be reset by this heating and replaced or overprinted by a new partial thermoremanent magnetization (pTRM). Thus, the clasts will now contain two components of magnetization – a low unblocking temperature component that will be parallel to the Earth's magnetic field at the time of cooling, and the original high unblocking temperature magnetization that will have random orientations from clast to clast. The emplacement temperature (T_e) of the lithic clasts can, therefore, be determined by progressive thermal demagnetization of the components of magnetization present within the clast. The estimate of T_e is the temperature above which the overprinted magnetization is removed and the

randomized high temperature magnetization is uncovered (e.g., McClelland and Druitt, 1989; Bardot, 2000).

Emplacement temperature validation

The palaeomagnetic technique may give erroneous results if the magnetic mineralogy of a lithic clast has altered by being heated, either during the eruption or during the laboratory experiment. Alteration of the ferromagnetic mineralogy of a lithic clast may also have occurred post-eruption during hydrothermal alteration of the deposits, and by low temperature diagenesis and weathering. The growth of a new magnetic phase during the eruption or during later alteration or laboratory heating could produce a chemical remanent magnetization (CRM) which would parallel the Earth's magnetic field at the time of alteration and may partly or completely replace the existing magnetization (Bardot and McClelland, 2000). The low unblocking temperature component in some samples could therefore have two origins; thermal activation (pTRM), which cannot exceed the T_e, or a CRM retained in newly formed or chemically altered grains resulting from alteration events. A secondary CRM may not demagnetize in the laboratory until the Curie temperature of the new magnetic phase, and this temperature would not be related to the emplacement temperature of the deposit (McClelland et al., 2004). In order to test the reliability of the emplacement temperature estimates, we monitored the variation of magnetic susceptibility with temperature to determine the Curie temperature (T_c) of the magnetic-mineral assemblages in the lithic clasts. To determine if the ferromagnetic

mineralogy of the lithic clasts was altered during syn- or post-eruption processes, the mineralogy of lithic clasts was compared with corresponding country rock samples.

An additional complication arises from the possible presence of Viscous Remanent Magnetisations (VRM). This is the magnetization that is gradually acquired by very small magnetic grains with very short relaxation times – they tend to rapidly realign with the most recent magnetic field, and yield a low-temperature component of magnetization that parallels the most recent field and can mask older components of magnetization. A VRM can be removed by thermal demagnetization at a specific time-temperature combination related to that at which the rock acquired the VRM. In essence this means that if the rock acquired a VRM over a period of 780,000 years (the time since the last magnetic reversal) we would need to heat it to a substantially higher temperature on a laboratory time scale (50 minutes) to remove it. This means that there is a lower limit on the emplacement temperature that we can determine using the palaeomagnetic technique, and for rocks older than 780,000 years this has been determined empirically to be 163°C (Bardot and McClelland, 2000). We have chosen to be conservative, given that there will also be some error on the temperature settings in our furnace (±10°C), and have not attributed any geological significance to components fitted below 180°C.

Methods

Sampling strategy

230 The sampling of the lithic clasts followed that outlined by McClelland and Druitt (1989)
231 and Bardot (2000). Given that the clasts were irregularly shaped, rigid plastic plates were
232 glued onto the surface of *in-situ* clasts and the strike and dip of the plate was recorded.
233 This was done so that we would have a perfectly flat surface for precisely orienting the
234 clasts. Clasts ranged in size from 4 to 24 cm diameter. Cores with a diameter of 1.9 cm
235 were drilled from Orapa A/K1 basalt clasts. Standard 2.5 cm diameter cores were drilled
236 from Venetia K1 and K2 clasts because they possessed weaker NRMs. Multiple core
237 specimens were obtained from individual lithic clasts to detect any magnetic
238 inhomogeneity or thermal gradients within the samples.
239
240 In the Orapa A/K1 pipe 110 basalt lithic clasts were sampled from the north pipe (NPK)
241 and the south pipe (SVK and talus breccias; Fig. 1a and 2a). Fifty five basalt lithic clasts
242 were sampled from the NPK from two localities at depths of 155 m and 140 m below
243 present surface (Sites 1 and 2 respectively; Fig. 1a and 2a). Five clasts were sampled from
244 talus breccias (Site 3; 95 m below present surface (bps)). Eight clasts were sampled from
245 inner crater SVK deposits at Site 4 (110 m bps) and 42 clasts from Site 5 (140 m bps). All
246 samples are tholeiitic Stormberg Formation basalt of Jurassic age. They are generally fine-
247 to medium-grained, holocrystalline and feldspar-phyric, with a seriate groundmass of
248 feldspars and pyroxenes. The feldspars exhibit embayed grain boundaries and breakdown
249 to oxides and the groundmass is altered to clay and chlorite.
250
251 Thirty-five lithic clasts were collected from the K1 and K2 pipes, Venetia mine. Thirty-
252 three clasts were collected from the two main lithofacies in K2: 28 from the matrix-

supported volcaniclastic kimberlite breccias (mVKBr) in K2 West and 5 from the massive volcaniclastic kimberlite deposits (MVK) in K2 East (Fig. 1b and 2b). Because the incorporation of lithic clasts can significantly cool pyroclastic mixtures (Marti et al., 1991) only localities with <35 vol.% lithic clasts were chosen for sampling. Sampling localities (Fig. 1b) aimed to provide a good radial and azimuthal spread, collecting six to eight clasts from a site spread over 5 to 10 m of outcrop. Sites 1 to 8 are exposed at 90 m bps, and sites 9 and 10 at 75 m bps (Fig. 1b). Two clasts were collected from MVK deposits in K1 (Site 1; Fig. 1c) at a depth of 170 m below present surface. Amphibolite gneiss clasts (13 clasts) were preferentially taken because they are the most likely to carry a strong and stable magnetization due to a suitable ferromagnetic mineral content and a competent massive structure. At some localities amphibolite clasts were scarce and biotite gneiss (5 clasts) and garnetiferous biotite schist (5 clasts) were sampled instead. Three argillite clasts, two basalt clasts, and seven clasts of Proterozoic dolerite were also sampled. At sites 6 and 7 there were no clasts that could be sampled.

Laboratory methods

Measurements of the natural remanent magnetization (NRM) were made in a magnetically shielded laboratory using a 2-G Enterprises cryogenic magnetometer. The samples were demagnetized using a Magnetic Measurements thermal demagnetizer with a residual field less than 50 nT in heating steps of 20°C or 40°C until the remaining intensity was less than 5% of the NRM. Occasionally more detailed steps were used where demagnetization occurred in a narrower temperature window. Demagnetization results were visually

inspected using orthogonal vector component plots (Zijderveld, 1967) and stereographic projections. Remanence directions were determined from stable end-points using principal component analysis (Kirschvink, 1980). Magnetic components were considered stable where they were defined by at least three points on vector component diagrams and had a maximum angular deviation (MAD) not exceeding 15°. Statistical analysis of the magnetization components and directional data were evaluated using Fisher (1953) spherical statistical parameters. The significance of groupings of vector components from each site was assessed using Watson's (1956) test for randomness.

The Curie temperature T_c of representative samples was determined by taking measurements of low-field susceptibility versus temperature, using a Agico KLY-2 Kappabridge magnetic susceptibility meter with furnace attachment, on 1–2 cm^3 of powdered sample taken from lithic clasts prior to thermal demagnetization. Measurements of susceptibility were made every 15–20 s as the sample was heated from 40–700°C, and then as it cooled back to 40°C, with a typical heating-cooling cycle taking about 2 hours. The Curie temperatures were determined using the inverse-susceptibility method of Petrovský and Kapička (2006). Polished sections were analysed using back-scattered imagery on a JEOL JSM-840A scanning electron microscope (SEM) and energy dispersive X-ray spectroscopy (EDS) using an Oxford Instruments ISIS 300 system.

Results

Orapa A/K1 kimberlite pipe, Botswana

The 110 basalt samples displayed NRM intensities from 0.20 to 48.7 amperes/meter (A/m). North pipe (NPK) samples displayed the highest intensities (1.05 to 48.7 A/m); with the majority displaying intensities >20 A/m. The lowest NRM intensities are displayed by talus breccia samples (<1 A/m). Fifty six samples were fully demagnetized after the 590°C heating step with the remaining samples demagnetized over heating steps between 600 and 700°C, indicating that the samples contain ferromagnetic grains with T_c >590°C. All samples exhibited stable behaviour during thermal demagnetization and displayed well-defined (MAD<15°) single or two-component magnetizations. Homogeneous thermal demagnetization behaviour is displayed between samples taken from the same clast in all but three clasts – where different emplacement temperature estimates were obtained from the rim and interior of the clasts.

Thermal demagnetization behaviour

Representative thermal demagnetization data for north pipe (NPK) and south pipe (SVK and talus breccias) samples are shown in Fig. 3. Groupings of magnetization directions on equal-area stereonets are shown in Fig. 4; statistical parameters are detailed in Table 1. Well-defined emplacement temperature determinations are obtained from clasts where two components of magnetization are identified through thermal demagnetization. In clasts where the primary magnetization has been overprinted by thermal activation (pTRM) of the magnetism, the two components are separated by a change in the direction of the magnetization, which occurs at the emplacement temperature. This behaviour is depicted

322 in Figs. 3a and 3b for samples AK1-38a1 and AK1-51a1 respectively (SVK; Site 5). In
323 sample AK1-38a1 (Fig. 3a) the initial magnetic vector points northwest (D = 330.5°) and
324 upwards (I = -60.6°). As demagnetization progresses (up to 240°C) the declination of the
325 vector rotates westwards and the inclination steepens. At subsequent heating steps the
326 direction of the vector remains similar, but the intensity decreases until the sample is fully
327 demagnetized between 570 and 590°C. These changes in the magnetization vector are
328 mapped by two separate lines. All points between room temperature and 240°C can be
329 fitted by a well-defined line (MAD = 2.9°) with a direction (D = 342.3°, I = -54.9°) that is
330 similar to the Cretaceous Earth's field direction (D = 350°, I = - 69°) for the region
331 (Hargreaves and Onstott, 1980). The points from 280°C to the origin of the plot lie on a
332 high-temperature line (MAD = 10.0°) with a direction (D = 245.1°, I = -65.9°) that is
333 different to that of the low-temperature component and the Cretaceous Earth's field
334 direction. This line represents the original magnetization of the clast which has moved to a
335 different orientation during transport in the deposit. An emplacement temperature (T_e)
336 estimate uses the temperature range between the last point on the low-temperature line and
337 the first point on the high-temperature line, in this case T_e = 240–280°C. In another
338 example AK1-51a1 (Fig. 3b) all points from room temperature to 360°C lie on a low-
339 temperature line with a direction (D = 359.6°, I = -32°) that is similar to the Cretaceous
340 direction, and all points from 400°C to the origin lie on a line with a direction (D = 291.7°,
341 I = -17.4°). In this case the emplacement temperature estimate is 360–400°C. We define
342 this demagnetization behaviour as 'type-1'. Three clasts display a variation in T_e estimates
343 between specimen cores taken from the interior and exterior of the clast. Sample AK1-
344 25a1 (Fig. 3c) taken from the exterior of the clast displays a two-component magnetization

345 with the separation of the two-components occurring at T_e = 280–320°C. In sample AK1-
346 25a2 (Fig. 3d) taken from the interior of the clast only a single component is present which
347 is identical to the high-temperature component of the exterior sample. This is the original
348 magnetization of the clast and indicates the core has not been heated above the minimum
349 temperature which can measured by palaeomagnetic methods.
350
351 If lithic clasts are heated to temperatures greater than the maximum Curie temperatures (T_c)
352 of the minerals they contain, the original magnetization will be completed overprinted by a
353 new pTRM component, and the magnetization will be a single-component parallel to the
354 Earth's magnetic field. In these examples the maximum T_c of the minerals will provide
355 minimum emplacement temperature estimates. This is defined as 'type-2' behaviour and
356 two examples with different maximum T_c are shown in Fig. 3e, f. Sample AK1-76b2 (Fig.
357 3e) is fully demagnetized between 660°C and 680°C and a single component of
358 magnetization (D = 1.9°, I = -67.4°) is defined by a well-fitted line (MAD = 4.5°) through
359 all data points from room temperature to the origin. The single-component (D = 337.2°, I =
360 -71.4°) in sample AK1-101a2 (Fig. 3f) is fully demagnetized between 570 and 590°C.
361 Both directions are similar to the Cretaceous Earth's field direction and the samples provide
362 minimum T_e estimates of >660°C and >570°C respectively. Samples where the natural
363 magnetic grain size distribution is extremely restricted and no grains with low unblocking
364 temperatures (T_{ub}) are present are defined as 'type-3' behaviour. No thermal overprint
365 would be recorded in these clasts if heated to temperatures less than the minimum T_{ub}. In
366 sample AK1-2a2 (Fig. 3g) no demagnetization occurs in heating steps up to 360°C, after
367 which the magnetization is removed between 400 and 590°C. Similar behaviour is shown

by sample AK1-5a1 (Fig. 3h) where demagnetization only occurs between 440 and 620°C. The magnetizations have a random direction and indicate the clasts have been emplaced at temperatures less than the minimum T_{ub}. The samples therefore provide maximum T_e estimates of <400°C and <440°C respectively.

All 110 basalt lithic clasts displayed well-defined single or two-component magnetizations of one of the three demagnetization behaviour types (types 1, 2 or 3). Twenty-five samples display a two-component magnetization (type-1) delineated by sharp changes in the direction of the magnetization vectors. Statistical grouping of the low-temperature components in these clasts is only observed for Site 5 (SVK; n = 23) with a mean direction (D = 330°, I = -43.9°, α95 = 12.2; Fig. 4a; Table 1) which is similar to the Cretaceous field direction. High-temperature components from the same clasts are scattered (Fig. 4b) indicating these are the original magnetizations of the samples. These samples were used to determine emplacement temperatures. Two samples from Site 4 displayed a two-component magnetization where the low-temperature components are different to the Cretaceous field direction. These are considered clasts which have either been moved within the deposit or have been emplaced at ambient temperatures, and the two-component magnetizations predate the emplacement. Due to this ambiguity, they have not been used to provide emplacement temperature estimates. Sixty-seven samples display a single-component (type-2) magnetization. All samples from NPK (n = 55; Sites 1 and 2) display single-component magnetizations that are significantly grouped and have a mean direction (D = 22.1°, I = -64.5°, α95 = 4.2°; Fig. 4c; Table 1) sub-parallel to the Cretaceous field direction. These are interpreted to have been emplaced at temperatures greater than the

Curie temperature of the minerals present. The remaining type-2 behaviour clasts (n = 12) exhibit single-component magnetizations that have random directions. These samples should acquire a pTRM component parallel to the Cretaceous field direction because of the well-distributed range of blocking temperatures. These are clasts interpreted to have been emplaced at ambient temperatures (i.e. the single-component is the original magnetization of the clasts which predates the eruption of the pipe). No groupings of single-component and two-component magnetizations are observed at Site 3 (talus breccias; Fig. 4d) and Site 4 (SVK; Fig. 4e) and these deposits are interpreted to have been emplaced at ambient temperatures. Eighteen samples display type-3 behaviour single-component magnetizations with restricted blocking temperature spectra where no low-T_{ub} grains are present. A thermal overprint would not be recorded in these clasts if they were emplaced at temperatures less than the minimum $T_{ub.}$ Therefore, where the overprint in these clasts does not parallel the Cretaceous field direction, the clasts provide minimum T_e estimates.

K2 and K1 pipes, Venetia Mine, South Africa

The thirty-five collected samples displayed weak remanent magnetizations with NRM intensities ranging from 0.043 to 85 mA/m. The majority exhibited intensities of < 1 mA/m. A well-distributed range of NRM intensities is displayed by amphibolite, biotite gneiss, argillite, and basalt clasts, with amphibolite samples showing both the lowest (0.043 mA/m) and highest (85 mA/m) measured NRM. All five garnetiferous biotite schist (GBS) samples displayed NRM intensities < 0.5 mA/m. Dolerite clasts displayed stronger intensities up to 82 mA/m, with five of the seven dolerite clasts displaying intensities > 10

mA/m. Twenty-four samples displayed stable magnetic behaviour in which a single or two-component magnetization could be identified over a range of heating steps. Homogeneous thermal demagnetization behaviour is displayed between all cores taken from the same clast, except for biotite gneiss sample V53 from Site 4 (mVKBr) which gave conflicting T_e estimates. The remaining eleven samples displayed erratic magnetizations, with strongly fluctuating intensities, in which no stable magnetization components could be identified. This behaviour is observed in all clast lithologies but restricted to the most weakly magnetized samples (intensities < 0.5 mA/m), and probably results from low signal-to-noise ratios within the samples. Garnetiferous biotite schist (GBS) samples displayed the most erratic behaviour, exhibiting massive intensity spikes (increases) that occur throughout the demagnetization process. Considerable mineralogical alteration occurred in GBS clasts during the heating process and no samples from Site 10 were including in any emplacement temperature determinations.

Of the twenty four samples that provided acceptable demagnetization results sixteen samples were fully demagnetized to <5% of the original NRM intensity at a peak temperature of 590°C. The remaining eight samples experienced unstable behaviour during the heating process above ~400°C, most likely a result of mineralogical alteration. Low temperature components could be identified and fitted in these samples.

Thermal demagnetization behaviour

Representative thermal demagnetization data for samples displaying stable single or two-component magnetizations are shown in Fig. 5. Grouping of magnetization directions on equal-area stereonets is shown in Fig. 6; statistical parameters are detailed in Table 1. Nine samples display a well-defined two-component (type-1) magnetization. An example is depicted in Fig. 5a for sample V2a (amphibolite; Site 8). In this example all points between room temperature and 260°C can be fitted by a well-defined line (MAD = 8.1°) with a direction (D = 322.7°, I = 31.7°), which is similar to a Cambrian reference palaeomagnetic direction (D = 317.1°, I = 42.5°) for the Venetia area (Meert, 2003). The points from 300°C to the origin lie on a high-temperature line (MAD = 7.2°) with a direction (D = 68.3°, I = -11.4°), different from the low-temperature component. The emplacement temperature (T_e) estimate uses the temperature range between the last point on the low-temperature line and the second point on the high-temperature line, in this case T_e = 260–300°C. The remaining eight type-1 samples display a well-defined two-component magnetization but where the low-temperature component does not parallel the Cambrian field direction. An example is shown for Fig 5b for sample V34b (biotite gneiss; Site 8). In this case all points between room temperature and 420°C can be fitted by a well-defined line (MAD = 8.3°) with a direction (D = 358.3°, I = -63.1°) that does not parallel the Cambrian field direction, but, is parallel to the Mesozoic field direction for the region. All points between 460°C and the origin can be fitted by a high-temperature line (MAD = 5.0°) with a direction (D = 277.5°, I = -34.7°) that is different from both the low-temperature line and the Cambrian field direction. Hence three interpretations are possible: a) the clast may have been emplaced at elevated temperatures (420−460°C) within the deposit, with a Cambrian overprint direction, but then moved within the deposit after it had cooled, with

459 the overprint direction fortuitously rotating to a Mesozoic field direction; b) the two-
460 component magnetization may have pre-existed in the clast, and it was emplaced at ambient
461 temperature; or c) the clast was emplaced at elevated temperature, but the Cambrian
462 overprint has itself later been overprinted by a Mesozoic field direction. Such a Mesozoic
463 overprint would likely be of chemical origin, and hence the sample cannot be used to
464 estimate a Cambrian emplacement temperature. Given that eight of the nine samples with a
465 stable two-component magnetizations yield low-temperature components that parallel the
466 Mesozoic field direction this is our preferred interpretation.
467
468 Two samples displayed stable single-component (type-2) magnetizations. An example is
469 depicted in Fig. 5c for sample V60a (amphibolite; Site 5). In this example a single
470 magnetization vector is defined by a well-fitted line (MAD = 6.1°) through all data points
471 from room temperature to the origin. The direction of the line (D = 308.4°, I = 22.3°) is
472 similar to the Meert (2003) Cambrian reference palaeomagnetic direction, implying the
473 clast was emplaced at temperatures greater than the maximum Curie temperatures of the
474 minerals it contains (in this case T_e >560°C). In three samples the natural magnetic grain
475 size distribution is extremely restricted and no grains with low unblocking temperatures
476 (T_{ub}) are present (type-3 behaviour). This is illustrated in Figs. 5d, e for Site 1dolerite
477 samples V18b and V19a respectively. In these samples little or no demagnetization occurs
478 in heating steps below 460°C, after which 90 % of the magnetization is removed. In
479 sample V18b (Fig. 5d) over 90% of the remanent magnetization is lost in heating between
480 500 and 590°C. As a TRM can only be recorded by high-T_{ub} grains in these samples, no
481 thermal overprint would be recorded in these clasts if heated to temperatures less than the

minimum T_{ub}. In sample V19a (Fig. 4e) all points between 460°C and the origin lie on a well-fitted line (MAD = 5.0°) with a direction (D = 253.0°, I = 25.5°) which is sub-parallel to the Cambrian field direction. This implies the clast was emplaced at a temperature greater than the maximum Curie temperatures of the minerals it contained (T_e > 560°C). However, in sample V18b (Fig. 5d) the direction of the magnetization (D = 274.1°, I = -69.9°) is different to the Cambrian field direction, and, instead parallels the Mesozoic field direction. This may suggest that this clast has been completely overprinted with a Mesozoic direction. The remaining ten samples ("type-4" behaviour) display a restricted range of blocking temperatures where no high-T_{ub} grains are present. This behaviour is independent of clast type. Representative samples displaying this behaviour are shown in Figs. 5f, g for samples V10a (argillite; Site 1) and V30a (biotite gneiss; Site 3) respectively. In these samples 80% of the remanent magnetization is removed by heating to 220–340°C. Well-defined lines can be fitted to a low-T_{ub} component, but no high-T_{ub} components can be defined after 80% of the remanence is removed because the signal-to-noise ratio becomes too low. Some samples are completely demagnetized at temperatures as low as 300°C (e.g. V10a; Fig. 5f) which indicates no ferromagnetic grains with T_{ub} >300°C are present. However, only one of these samples yields an over print direction that is not parallel to the Mesozoic field. In Site 1 amphibolite sample V23a (Fig 5h) a well-defined (MAD = 9.6°) component with a direction D = 47.6°, I = 61.4° can be fitted to all points from room temperature to 340°C, after which the magnetization of the sample becomes erratic.

For the Venetia samples the emplacement temperature estimations are complicated by the lack of samples displaying stable magnetic behaviour, preventing unbiased statistical analysis of the magnetization components. As noted above there is a prevalence of low-temperature components that parallel the Mesozoic field direction (Fig. 6a; Table 1). They are likely of chemical origin and these samples cannot be used for emplacement temperature determinations. This leaves us with only 4 samples, which have overprint directions that might be Cambrian in age: one type-1 (V2a); one type-2 (V60a); one type-3 (V19a); and one type-4 (V23a). When these are combined they yield a mean-direction declination of 308° and a mean inclination of 46° (Fig. 6b; Table 1), but the statistical parameters are very poor, only just passing the Watson (1956) test for non-randomness (Table 1). Nevertheless these four samples indicate emplacement temperatures of 260°C to >560°C. The values are similar to that obtained at Orapa, and are taken to be supportive of a range of emplacement temperatures of the kimberlite lithofacies, rather than being diagnostic in their own right.

Rock magnetism results

Spurious emplacement temperature estimates may result from lithic clasts where the magnetic mineralogy has been altered during or after emplacement. Newly formed or chemically altered grains will acquire a chemical remanent magnetization (CRM) parallel to Earth's magnetic field which may partly or completely overprint the existing magnetization. The unblocking temperatures of these components may not coincide with T_e but instead record the Curie temperatures (T_c) of new grains formed in a later (possibly

low-temperature) alteration event. To test the reliability of the emplacement temperature results we determined the range of T_c values by measuring the variation in magnetic susceptibility with temperature in 32 powdered samples from lithic clasts which provided T_e estimates from the thermal demagnetization study. The Curie temperatures were determined using the inverse-susceptibility method of Petrovský and Kapička (2006).

Representative magnetic susceptibility-temperature curves for 9 basalt lithic clasts sampled from Orapa A/K1 and 2 amphibolite samples from Venetia K2 are shown in Fig. 7; Demagnetization vector plots are also shown for three samples with T_e estimates ranging from 240–280°C to 360–400°C. We find most basalt samples (n = 26) are dominated by magnetite or Ti-poor titanomagnetites ($x_{Ti} \leq 0.1$) with T_c values of 559-595°C (e.g., Fig. 7a, b, and f, h). Little or no alteration has occurred during heating or cooling of the samples, although 11 samples show a higher susceptibility (but no change in T_c) after the experiment (e.g., Fig. 7j, l). This is interpreted to result from the annealing of defects within the crystal lattice of ferromagnetic minerals during heating (Bardot, 1997). The remaining basalt samples (n= 4) with T_c values of 595-613°C could result from the oxidation of magnetite to maghemite (or titanomagnetite to titanomaghemite) during the laboratory heating. The main ferromagnetic minerals within amphibolite samples (n = 2) is titanomagnetite ($x_{Ti} \sim 0.2$) with T_c values of ~500°C (Fig. 6l, m). No spurious T_c values are observed to coincide with the emplacement temperature estimates obtained during thermal demagnetization which supports the validity of the emplacement temperature results.

Petrography and textural relations

The basalt lithic clasts contain ilmenite and titanomagnetite grains in roughly equal proportions (total proportion 5–15%). Grain diameters vary from <1 μm to ~200 μm. Ilmenite typically occurs as elongate grains (<100 μm length) and titanomagnetites as subhedral to euhedral grains (10–200 μm diameter). Titanomagnetites invariably display coarse or fine ilmenite lamellae along {111} crystallographic planes, and occasionally contain inclusions of ilmenite with irregular or sharp boundaries parallel to the crystallographic axes (Fig. 8a, b). The host titanomagnetite is enriched in Fe with compositions approaching magnetite. These features are typical of deuteric oxidation of host titanomagnetite grains (Ulvospinel-Magnetite solid solution) in igneous rocks (Haggerty, 1991). The intergrowth textures dramatically reduce the effective grain size of the host titanomagnetites (Fig. 8c, d) and it is likely a proportion of the thermal remnant magnetization (TRM) is carried by these magnetite or Ti-poor titanomagnetite intergrowth grains. These textures are mirrored in country rock samples (Fig. 8e, f), although finer grained and skeletal titanomagnetites are observed in samples from basalt flow tops. Collectively these observations indicate that there is no evidence of pervasive hydrothermal alteration of primary igneous ferromagnetic grains or the growth of new ferromagnetic species in the lithic clast samples. The oxides observed under the SEM, however, are larger than those which typically carry stable magnetic remanence, which are normally in the sub-μm size range and hence below the resolution of the SEM, but the fact that original igneous textures are preserved gives us confidence that the primary magnetic mineralogy is likely also preserved within the lithic clasts.

573 The amphibolite gneiss lithic clasts in Venetia K1 and K2 are upper amphibolite
574 metamorphic facies rocks of the Venetia Klippe unit (Barton et al., 2003). They show
575 compositional variability but typically display granoblastic textures containing hornblende
576 ± garnet + biotite ± feldspar ± quartz + ilmenite. Fe-Ti oxide proportions vary from <1% to
577 3%. Oxides occur as acicular grains in garnets and biotites (<100 μm length), or as larger
578 (≤300 μm) anhedral inclusions within hornblende grains (Figs. 8g, h). The grains are
579 typically host illmenite grains with bladed intergrowths of rutile and titanite, or fine grained
580 mottled intergrowths of Ti-poor titanomagnetite, rutile and illmenite. These textures and
581 assemblages are mirrored in samples of *in situ* amphibolite country rock. Therefore little
582 alteration of the metamorphic and ferromagnetic mineralogy of the lithic clasts is
583 considered to have occurred during their emplacement. The paucity of magnetite and
584 titanomagnetite in the samples accounts for weak magnetizations observed in the lithics.
585
586 **Emplacement temperatures and their interpretation**
587
588 Given the relative paucity of data from the Venetia pipes we focus on the results from the
589 Orapa A/K1 kimberlite pipe, Botswana. Palaeomagnetically determined T_e estimates
590 determined from individual lithic clasts are shown in Fig. 9. Single-component (type-2; n =
591 55) magnetizations in NPK basalt clasts provide minimum T_e estimates of >570°C to
592 >660°C for vent-filling pyroclastic breccias (Fig. 9a). Maximum T_e estimates of <180°C
593 (which is the lower limit of the palaeomagnetic method for these samples) are provided by
594 randomly orientated single-component and low-temperature component magnetizations (n
595 = 13) in SVK and talus breccia samples (Fig. 9b). These are interpreted to have been

596 emplaced at ambient temperatures. Well-defined two-component magnetizations (n = 23)
597 provide T_e estimates of 200–440° for lithic clasts within inner crater SVK deposits (Fig.
598 9b).
599
600 The results from NPK samples provide minimum deposit equilibrium temperatures (T_{dep}) of
601 >570°C which implies that the NPK is a primary pyroclastic deposit emplaced at
602 significantly elevated temperatures, as proposed by Field at al. (1997) based on field and
603 petrographic evidence. NPK rocks contain the typical metamorphic alteration assemblage
604 of serpentine and diopside which is constrained to be formed at temperatures <400°C
605 (Stripp et al., 2006). This lower estimate on the emplacement temperature of the deposits is
606 consistent with the deposits being emplaced at higher temperature (according to the TRM
607 results) with olivine, as the major component of the deposits, being stable. Later as the
608 deposits cooled down in a hydrothermal system olivine is replaced by serpentine to
609 generate the lower temperature assemblage. T_e estimates for SVK samples of <180°C in
610 talus breccias and <180°C to 200–440°C in volcaniclastic breccias implies that clasts were
611 emplaced in the south pipe at both ambient and elevated temperatures. This indicates both
612 epiclastic and pyroclastic depositional processes occurred in the south pipe. The result
613 from talus deposits is consistent with emplacement by epiclastic processes around the
614 margin of the pipe, as proposed by Field et al. (1997). Volcaniclastic breccias emplaced at
615 ambient temperatures within the inner crater are consistent with emplacement as rock-fall
616 and debris-flow deposits (Field et al., 1997; Gernon et al. 2009a). Clasts emplaced at
617 elevated temperatures (Site 5; Fig.1a and 2a) are located within a laterally extensive, 15–20
618 m thick kimberlite pyroclastic flow unit described by Gernon et al. (2009b). The unit lies

619 unconformably over crater-filling deposits, which postdate the eruption of the north pipe.
620 Gernon et al. (2009b) infer that the pyroclastic flow originated from a neighbouring
621 kimberlite pipe.
622
623 **Volcanological implications**
624
625 Results from Orapa A/K1 provide minimum T_{dep} values of >570°C for vent-filling
626 pyroclastic rocks. These samples were heated to temperatures greater than the Curie
627 temperatures of the minerals present and are observed to have reached thermal equilibrium
628 within the deposit. It is inferred that most, if not all, of the lithic clasts will have been
629 incorporated into the vent-filling pyroclastic deposits at ambient temperatures because the
630 conduit wall rock will have been cold prior to onset of volcanism. The mixing of cold lithic
631 clasts with erupting kimberlite magma will cool the erupting pyroclastic mixture (Marti et
632 al., 1991) as heat is shared out between the juvenile kimberlite pyroclasts and lithic clasts.
633 An idealised equilibrium temperature of the erupting mixture of pyroclastic and lithic
634 components, T_M, can be calculated from the heat conservation equation:
635
636 $$T_M = \frac{C_K T_K (1-x) - x C_L T_L}{C_L x + C_K (1-x)},$$
637
638 where T_K is the temperature of the kimberlite pyroclasts (assumed to be similar to
639 kimberlite magmatic temperatures of 1273-1473 K (Ferdochouk and Canil, 2004; Mitchell,
640 2008; Sparks et al., 2009), T_L is the initial temperature of the lithic clasts (293 K), x is the
641 mass fraction of lithic clasts entrained in the mixture, C_K is the specific heat capacity of

642 kimberlite pyroclastics ($C_{olivine}$ at 1000 K = 1150 J kg^{-1} K^{-1}; Gillet et al., 1991), and C_L is the
643 specific heat capacity of lithic clasts (C_{basalt} at 800 K = 1100 J kg^{-1} K^{-1}; Bouhifd et al.,
644 2007). The conversion of lithic clast volume to weight % was made using standard
645 densities for lithic clasts (ρ_{basalt} = 2900 kg m^{-3}), and kimberlite pyroclasts ($\rho_{olivine}$ = 3270 kg
646 m^{-3}). The average proportion of lithic clasts within vent-filling pyroclastic breccias is ~10–
647 20% (Walters et al., 2006; Brown et al., 2009). The bulk mixing of a juvenile magmatic
648 component with 10–20 % cold lithic clasts (x = 0.08–0.16) would reduce the temperature of
649 the mixture from magmatic temperatures of 1000°C to ~920-850°C. These values can be
650 considered maximum estimates of the T_{dep} of vent-filling deposits and therefore the vent-
651 filling deposits in A/K1 could have been 200–300°C hotter than the TRM estimates
652 (>570°C). T_e estimates for individual lithic clasts within the pyroclastic flow deposit in the
653 Orapa south pipe crater range from 200–440°C. The average lithic content of the
654 pyroclastic flow deposit is ~30% (Gernon et al., 2009b) and the ideal equilibrium
655 temperature for a mixture of juvenile magma at 1000°C and 30 vol.% (x = 0.25) cold lithic
656 clasts is ~760°C. The deposit is interpreted as a lithic breccia deposited rapidly upon
657 deceleration of a pyroclastic flow (Gernon et al., 2009b). The scatter in the observed T_e
658 estimates can be explained if some of the lithic clasts do not equilibrate with the flow
659 temperature during rapid transportation. Since the clasts were originally cold and were
660 heated up in the deposit, the upper T_e estimates of 400–440°C most closely represent the
661 equilibrium temperature of the deposit. Further cooling of the pyroclastic flow from source
662 temperatures of ~760°C to deposit equilibrium temperatures of 400–440°C can be
663 explained by air entrainment during transport, and does not necessitate the input of water
664 (Sparks et al., 1978).

The amount of cooling due to the incorporation and vapourisation of water into the pyroclastic flow can be determined using the heat balance equation:

$$T_{dep} = T_M - \left[\frac{yC_{LW}(T_{100}-T_W)+yL_W+yC_{VW}(T_K-T_{100})}{C_M(1-y)}\right],$$

where T_M is the initial temperature of the pyroclastic mixture, T_W is the initial water temperature (293 K) which will be heated to boiling point T_{100} (373K), y is the mass fraction of water, L_W is the latent heat of vaporization of water (2.3×10^6 J kg^{-1}), C_{LW} is the specific heat capacity of liquid water (4228 J kg^{-1} K^{-1}), C_M is the heat capacity of the pyroclastic flow (assumed to be similar to kimberlite pyroclasts; $C_{olivine}$ at 1000 K = 1150 J kg^{-1} K^{-1}), C_{VM} is the specific heat capacity of steam (2040 J kg^{-1} K^{-1}). Cooling of approximately ~300°C from eruption to deposit equilibrium temperatures would require 10 wt. % liquid water.

Conclusions

Thermoremanent magnetism studies of lithic inclusions have successfully differentiated the emplacement temperatures of a variety of volcaniclastic lithofacies preserved within the Cretaceous Orapa kimberlite pipes (Fig. 10). Data from the Cambrian-aged Venetia pipe are of a much lower quality, but they do not contradict the results from Orapa. Obtained T_{dep} values are consistent with the field evidence of the various deposits (Field et al., 1997;

688 Brown et al., 2009; Gernon et al., 2009a). T_{dep} estimates for pyroclastic deposits are
689 consistent with previous estimates of kimberlite emplacement temperatures (≤340°C;
690 Sosman 1938; Watson 1967; McFadden, 1977; Stasiuk et al., 1999). The T_{dep} values
691 obtained for pipe-filling pyroclastic deposits (260–300°C to >570°C) are similar to the
692 emplacement temperatures of extrusive pyroclastic rocks erupted from more silicic volcanic
693 systems (Hoblitt and Kellogg, 1979; Banks and Hoblitt, 1981; Kent et al., 1981; Cioni et
694 al., 2004; McClelland et al., 2004; Scott and Glasspool, 2005). Pyroclastic deposits
695 become welded at high temperatures and this is particularly common in pyroclastic deposits
696 of low-viscosity magmas (Sumner 1998). Welding textures have recently been recognised
697 in some rocks in Venetia K2 pipe (Brown et al., 2008), providing further evidence of high
698 emplacement temperatures for some kimberlite pyroclastic deposits. Low T_{dep} estimates for
699 clasts in the SVK and talus breccias (<180°C), which show a single-component
700 magnetization, are consistent with emplacement at ambient temperatures by epiclastic
701 processes (rock fall and debris flow; Fig. 10; see Field et al., 1997; Gernon et al., 2009a).
702
703 Many kimberlite pipes exhibit evidence for multiple phases of eruptive activity (e.g., nested
704 and cross-cutting pyroclastic and breccia units (Venetia K2 and K1; Kurszlaukis and
705 Barnett, 2003; Brown et al., 2009; Koffiefontein, South Africa, Naidoo et al., 2004). The
706 periods between these phases of activity are unknown, but the presence of clasts with two-
707 component magnetizations may indicate that individual kimberlite pipes are active over
708 limited periods. The well-defined, two-component magnetizations could only have been
709 acquired if they had cooled in a stationary position, after the deposits had completely
710 stabilised and were not subsequently rotated or moved. Cooling times by conduction for

711 kimberlite pipe fills are estimated at decades to centuries (Sparks et al., 2006), thus, late-
712 stage disruptive volcanic activity must have taken place while the deposits were still hot or
713 after the deposits had cooled and lithified (by diagenesis and serpentinisation). The results
714 from are consistent with high temperature mineral assemblages of serpentine-diopside-
715 calcite-chlorite observed in these deposits, which indicate temperatures of 300-340°C
716 (Stripp et al., 2006).
717
718 The T_{dep} estimates for the pyroclastic deposits allow some constraints to be placed on the
719 eruption dynamics of studied kimberlite pipes. Minimum T_{dep} values of 260–300°C to
720 >570°C in the Venetia and Orapa pipes are consistent with volatile-driven explosive
721 eruptions. The temperatures of kimberlite magmas is now thought to be in the range of
722 1200-1000°C (Ferdochouk and Canil, 2006; Mitchell, 2008; Sparks et al., 2009). The
723 incorporation of 10–20% cold lithic clasts would cool the source pyroclastic mixture from
724 magmatic temperatures to 920–850°C. Therefore the actual temperatures of the primary
725 components of the vent-filling deposits may have been 200–300°C higher than the TRM
726 estimates. Similarly the Orapa south pipe contains a pyroclastic flow deposit with, on
727 average, 30 % lithic clasts (Gernon et al., 2009b) and so the original pyroclastic component
728 may have hotter by up to 300°C than the TRM estimates. The amount of cooling from
729 magmatic temperatures to the estimated deposit temperatures is typical of many other
730 pyroclastic deposits worldwide, and can be explained by the entrainment and heating of air
731 and cold lithic material. It is difficult to reconcile these elevated emplacement temperatures
732 with phreatomagmatic explosivity. Explosive interaction of ground or surface water with
733 rising magmas commonly cools erupting flows close to ambient (Thomas, 1993; Bardot et

734 al., 1996). Quantitative measurements of the emplacement temperatures of
735 phreatomagmatic deposits indicate values of <140°C (Thomas, 1993; Bardot et al., 1996;
736 Porreca et al., 2008) to as much as 275°C (De'Gennaro et al., 1996). Low temperatures in
737 phreatomagmatic deposits are also suggested by many features such as the inclusion of
738 uncharred wood in phreatomagmatic deposits (e.g., Giordano et al., 2002) and by the
739 plastering of wet ash onto obstacles (e.g., Cole et al., 2001). However, we stress that our
740 findings do not rule out phreatomagmatic explosivity during kimberlite eruptions.
741
742 This research demonstrates that thermoremanent studies of lithic inclusions can
743 successfully differentiate between epiclastic and pyroclastic deposits within ancient
744 kimberlite crater-fill successions. This may have important economic implications for the
745 mining and exploration of kimberlite bodies - not all deposits preserved within a volcanic
746 crater above a kimberlite pipe may be sourced directly from that pipe.
747
748 **Acknowledgements**
749
750 GF was supported by a Natural Environment Research Council Open CASE studentship
751 (NE/F008457/1). All authors acknowledge funding and support by De Beers Consolidated
752 Mines and Debswana. S. Trickett is thanked for collecting some of the Orapa A/K1
753 samples for preliminary study, and B. Buse is thanked for providing basalt country rock
754 samples for petrological study. M. Tait, A. Mynama and V. Pitt are thanked for on-site
755 support during fieldwork at Venetia mine. We thank O. Mashabila, T. Tlhaodi and P.
756 Kesebonye for their assistance with logistics and fieldwork at Orapa. Randy Enkin, Adrian

757 Muxworthy, Greig Paterson, & Kelly Russell are thanked for comments and reviews that
758 greatly helped us in clarifying aspects of this manuscript. RSJS acknowledges a Royal
759 Society-Wolfson Merit award and a European Research Council Advanced grant.
760
761 Aramaki S, Akimoto S (1957) Temperature estimate of pyroclastic deposits by natural
762 remanent magnetism. Am J Sci 255:619–627
763 Banks NG, Hoblitt RP (1981) Summary of temperature studies of 1980 deposits. In:
764 Lipman, PW, Mullineaux DR, (eds) The 1980 eruptions of Mount St. Helens, Washington.
765 US Geol Surv Prof Pap 1250: 295–313
766 Bardot L (1997) Explosive volcanism on Santorini: palaeomagnetic estimation of
767 emplacement temperatures of pyroclastics. PhD thesis, University of Oxford, Oxford
768 Bardot L (2000) Emplacement temperature determinations of proximal pyroclastic deposits
769 on Santorini, Greece, and their implications. Bull Volcanol 61:450–467
770 Bardot L, McClelland E (2000) The reliability of emplacement temperature estimates using
771 palaeomagnetic methods: a case study from Santorini, Greece. Geophys J Int 143: 39–51
772 Bardot L, Thomas R, McClelland E (1996) Emplacement temperatures of pyroclastic
773 deposits on Santorini deduced from palaeomagnetic measurements: constraints on eruption
774 mechanisms. In: Morris A, Tarling DH (eds) Palaeomagnetism and tectonics of the
775 Mediterranean region. Geo Soc London Spec Pub 105: 345–357
776 Barton Jr JM, Barnett WP, Barton ES, Barnett M, Doorgapershad A, Twiggs C, Klemd R,
777 Martin J, Mellonig L, Zenglein R (2003) The geology surrounding the Venetia kimberlite
778 pipes, Limpopo Belt, South Africa: a complex interplay of nappe tectonics and granitoid
779 magmatism. S Afr J Geol 106:109–128

780 Bouhifd M, Besson P, Courtial P, Gérardin C, Navrotsky A, Richet P (2007)
781 Thermochemistry and melting properties of basalt. Contrib Mineral Petrol 153 (6):689–698
782 Brown, RJ, Buse, B, Sparks, RSJ, Field, M, 2008. On the welding of pyroclasts from very
783 low viscosity magmas: examples from kimberlite volcanoes. J Geol 116, 354-374
784 Brown RJ, Tait M, Field M, Sparks RSJ (2009) Geology of a complex kimberlite pipe
785 (Venetia K2 pipe, South Africa): insights into conduit processes during explosive ultrabasic
786 eruptions. Bull Volcanol 71: 95–112
787 Buse B, Schumacher JC, Sparks RSJ, Field M (2010) Growth of bultfonteinite and
788 hydrogarnet in metasomatized basalt xenoliths in the B/K9 kimberlite, Damtshaa,
789 Botswana: insights into hydrothermal metamorphism in kimberlite pipes. Contrib Mineral
790 Petrol. doi:10.1007/s00410-010-0492-4
791 Cioni R, Gurioli L, Lanza R, Zanella E (2004) Temperatures of the A.D. 79 pyroclastic
792 density current deposits (Vesuvius, Italy). J Geophys Res 109:B02207
793 Clement CR, Reid AM (1989). The origin of kimberlite pipes: an interpretation based on
794 the synthesis of geological features displayed by southern African occurrences. In: Ross J,
795 Jaques AL, Fergusan J, Green DH, O'Reilly SY, Danchin RV, Janse AJA (eds) Kimberlites
796 and related rocks. Sydney, Geol Soc Australia 632–646
797 Clement BM, Connor CB, Graper G (1993) Palaeomagnetic estimate of the emplacement
798 temperature of the long-runout Nevado de Colima volcanic debris avalanche deposit,
799 Mexico. Earth Planet Sci Lett 120:499–510
800 Cole PD, Guest JE, Duncan AM, Pacheco JM (2001) Capelinhos 1957-1958, Faial, Azores:
801 deposits formed by an emergent Surtseyan eruption. Bull Volcanol 63:204–220
802 Dawson J.B (1971) Advances in kimberlite geology. Earth Sci Rev 7:187–214

803 De'Gennaro M, Gialanella PR, Incoronato A, Mastrolorenzo G, Naimo D (1996)
804 Palaeomagnetic controls on the emplacement of the Neapolitan Yellow Tuff (Campi
805 Flegrei, Southern Italy). In: Morris A, Tarling DH (eds) Palaeomagnetism and tectonics of
806 the Mediterranean region. Geol Soc London Spec Pub 105:359–265
807 Downey WS, Tarney DH (1991) Reworking characteristics of Quaternary pyroclastics,
808 Thera (Greece), determined using magnetic properties. J Volcanol Geoth Res 46:143–155
809 Fedortchouk Y, Canil D (2004) Intensive variables in kimberlite magmas, Lac de Gras,
810 Canada and implications for diamond survival. J Petrol 45:1725–1745
811 Field M, Gibson JG, Wilkes TA, Gababotse J, Knutjwe P (1997) The geology of the Orapa
812 A/K1 kimberlite Botswana: further insight into the emplacement of kimberlite pipes.
813 Russian Geol Geophys 38:24–39
814 Field M, Scott Smith BH (1999) Contrasting geology and near-surface emplacement of
815 kimberlite pipes in South Africa and Canada. In: Gurney JJ, Gurney JL, Pascoe MD,
816 Richardson SH (eds) Proceedings of the 8th International Kimberlite Conference, Red Roof
817 Design, Cape Town 214-238
818 Fisher RA (1953) Dispersion on a sphere. Proc R Soc Lon Mat. A217: 295–305.
819 Gernon T, Field M, Sparks RSJ (2009a) Depositional processes in a kimberlite crater: The
820 Upper Cretaceous Orapa South Pipe (Botswana). Sedimentology 56:623–643
821 Gernon T, Fontana G, Field M, Sparks RSJ, Brown RJ, Mac Niocaill C (2009b) Pyroclastic
822 flow deposits from a kimberlite eruption: the Orapa South Crater, Botswana. Lithos
823 112S:566–578
824 Gillet P, Richet P, Guyot F, Fiquet G (1991) High-temperature thermodynamic properties
825 of forsterite. J Geophys Res 96(B7):11805–11816

826 Giordano G, De Rita D, Cas R, Rodani S (2002) Valley pond and ignimbrite veneer
827 deposits in the small-volume phreatomagmatic 'Peperino Albano' basic ignimbrite, Lago
828 Albano maar, Colli Albani volcano, Italy: influence of topography. J Volcanol Geoth Res
829 118:131–144
830 Haggerty SE (1991) Oxide Textures - A Mini-Atlas. In: Lindsley DH (ed) Oxide Minerals:
831 Petrologic and Magnetic Significance. Reviews in Mineralogy, vol 25. Mineralogical
832 Society of America, Washington, DC, 129–220
833 Hargreaves RB, OnStott TC (1980) Palaeomagnetic results from some South African
834 kimberlites, and their tectonic significance. J Geophys Res 85(B7):3387–3596
835 Hoblitt RP, Kellogg KS (1979) Emplacement temperatures of unsorted and unstratified
836 deposits of rock debris as determined by palaeomagnetic techniques. Geol Soc Am Bull
837 90:633–642
838 Kent DV, Ninkovich D, Pescatore T, Sparks RSJ (1981) Palaeomagnetic determination of
839 emplacement temperature of Vesuvius AD 79 pyroclastic deposits. Nature. 290:393–396
840 Kirschvink JL (1980) The least-squares line and plane and the analysis of paleomagnetic
841 data. Geophys J R Astron Soc 62:699–718
842 Kjarsgaard BA (1996) Kimberlite-hosted diamond. In: Eckstrand OR, Sinclair WD, Thorpe
843 RI (eds) Geology of Canadian Mineral Deposit Types. Geological Survey of Canada, vol.
844 8:560–568
845 Kurszlaukis S, Barnett W (2003) Volcanological and structural aspects of the Venetia
846 kimberlite cluster – A case study of South African kimberlite maar-pipe volcanoes. S Afr J
847 Geol 106:165–192

Kurszlaukis S, Büttner R, Zimanowski B, Lorenz V (1998) On the first experimental phreatomagmatic explosion of a kimberlite melt. J Volcanol Geoth Res 80:323–326

Lorenz V (1975) Formation of phreatomagmatic maar-pipe volcanoes and its relevance to kimberlite pipes. Phys Chem Earth 9:17–29

Lorenz V, Kurszlaukis S (2007) Root zone processes in the phreatomagmatic emplacement model and consequences for the evolution of maar-diatreme volcanoes. J Volcanol Geoth Res 159:4–32

Mandeville CW, Carey S, Sigurdsson H, King J (1994) Paleomagnetic evidence for high-temperature emplacement of the 1883 subaqueous pyroclastic flows from Krakatoa Volcano, Indonesia. J Geophys Res 99:9487–9504

McClelland EA, Druitt TH (1989) Palaeomagnetic estimates of emplacement temperatures of pyroclastic deposits on Santorini, Greece. Bull Volcanol 51:16–27

McClelland E, Wilson CJN, Bardot L (2004) Palaeo-temperature determinations for the 1.8-ka Taupo ignimbrite, New Zealand, and implications for the emplacement history of a high-velocity pyroclastic flow. Bull Volcanol 66: 492–513

McFadden PL (1977) A palaeomagnetic determination of the emplacement temperature of some South African kimberlites. Geophys J R Astron Soc 50:605–619

Meert JG (2003) A synopsis of events related to the assembly of eastern Gondwana. Tectonophysics 362:1–40

Marti J, Diez-Gil JL, Ortiz R (1991) Conduction model for the thermal influence of lithic clasts in mixtures of hot gases and ejecta. J Geophys Res 96(B13):21879–21885

Mitchell RH (1986). Kimberlites: Mineralogy, Geochemistry, and Petrology. Plenum Press, New York 442 pp

871 Mitchell RH (2008) Petrology of hypabyssal kimberlites: relevance to primary magma
872 compositions. J Volcanol Geoth Res 174:1–8
873 Naidoo P, Stiefenhofer J, Field A, Dobbe R, (2004) Recent advances in the geology of
874 Koffiefontein mine, Free State Province, South Africa. Lithos 76:161–182
875 Petrovský, E, Kapička, A. (2006). On determination of the Curie point from
876 thermomagnetic curves. J Geophys Res 111**,** B12S27, doi:10.1029/2006JB004507
877 Paterson GA, Roberts AP, Mac Niocaill C, Muxworthy AR, Gurioli L, Viramonté JG,
878 Navarro C, Weider, S (2010) Paleomagnetic determination of emplacement temperatures of
879 pyroclastic deposits: an under-utilized tool. Bull Volcanol 72:309-330
880 Phillips D, Kiviets GB, Barton ES, Smith CB, Viljoen KS, Fourie LF (1999) 40Ar/39Ar
881 dating of kimberlites and related rocks: problems and solution. Proceedings of the 7th
882 International Kimberlite Conference Cape Town, South Africa 677–687
883 Porreca, M., Mattei, M., Mac Niocaill, C., Giordano, G., McClelland, E., Funicello, R,
884 (2008). Paleomagnetic evidence for low-temperature emplacement of the phreatomagmatic
885 Peperino Albano ignimbrite (Colli Albani volcano, Central Italy). Bull Volcanol 70:877–
886 893
887 Scott AC, Glasspool IJ (2005) Charcoal reflectance as a proxy for the emplacement
888 temperature of pyroclastic flow deposits. Geology 33:589–592
889 Seggie AG, Hannweg GW, Colgan EA, Smith CB (1998) The geology and geochemistry of
890 the Venetia kimberlite cluster, Northern Province, South Africa. Proceedings of the 7th
891 International Kimberlite Conference, Cape Town, South Africa 1:750–756
892 Skinner EMW, Marsh JS (2004) Distinct kimberlite pipe classes with contrasting eruption
893 processes. Lithos 76:183–200

894 Sosman RB (1938) Evidence on the intrusion-temperature of peridotites. Am J Sci 35:353–
895 359
896 Sparks RSJ, Baker L, Brown RJ, Field M, Schumacher JC, Stripp G, Walters A (2006)
897 Dynamical constraints on kimberlite volcanism. J Volcanol Geoth Res 155:18–48
898 Sparks RSJ, Brooker RA, Field, Kavanagh J, Schumacher JC, Walter MJ, White J (2009)
899 The nature of erupting kimberlite melts. Lithos 112S:429–438
900 Stasiuk LD, Lockhart GD, Nassichuk WW, Carlson JA, (1999) Thermal maturity
901 evaluation of dispersed organic matter inclusions from kimberlite pipes, Lac de Gras,
902 Northwest Territories, Canada. Int J Coal Geol 40:1–25
903 Stripp GR, Field M, Schumacher JC, Sparks RSJ (2006) Post-emplacement serpentinization
904 and related hydrothermal metamorphism in a kimberlite from Venetia, South Africa. J
905 Metamorph Geol 24:515–534
906 Sumner JM (1998) Formation of clastogenic lava flows during fissure eruption and scoria
907 cone collapse: the 1986 eruption of Izu-Oshima Volcano, eastern Japan. Bull Volcanol
908 60:195–212
909 Thomas RME (1993) Determination of the emplacement temperatures of pyroclastic
910 deposits by theoretical and palaeomagnetic methods. PhD Thesis, University of Bristol,
911 Bristol
912 Walters A, Phillips J, Brown RJ, Field M, Gernon T, Stripp G, Sparks, RSJ (2006) The role
913 of fluidisation processes in the formation of volcaniclastic kimberlite: grain size
914 observations and experimental investigation. J Volcanol Geoth Res 155:119–137
915 Watson KD (1967) Kimberlites of Eastern North America. In: Wyllie PJ (ed) Ultramafic
916 and Related Rocks. John Wiley & Sons, Inc, New York 312-323

Watson GS (1956) A test for randomness of directions. Monthly Notices. Geophys J R Astron 7:160–161

Wilson L, Head JW III (2007) An integrated model of kimberlite ascent and eruption. Nature. 447:53–57

Wright JV (1978) Remanent magnetism of poorly sorted deposits from the Minoan eruption of Santorini. Bull Volcanol 41:527–544

Zijderveld JDA (1967) A.C. demagnetization of rocks: Analysis of results. In: Collinson DW, Creer KM, Runcorn K (ed) Methods in Palaeomagnetism.Elsevier, Amsterdam 254–286

Figure Captions

Figure 1. Simplified geological maps of the studied kimberlites, with major lithofacies identified and localities of samples indicated by crosses. **a** Summary geological map of the Orapa A/K1 kimberlite body (modified from Field et al., 1997 and Gernon et al., 2009a). The body comprises two steep-sided pipes (north and south). **b** Simplified geological map of the K2 kimberlite pipe, Venetia Mine, South Africa (from Brown et al., 2008). **c** Geological map of K1 kimberlite pipe, Venetia Mine, South Africa. **Inset**: map of southern Africa and locations of mines.

Figure 2. **a** Photograph of the Orapa A/K1 mine (looking south), showing the localities and stratigraphic context of the sampled deposits (sampling sites are numbered). The wall rock comprises Stormberg Formation basalts and Ntane Formation sandstones, the latter of

940 which crop out as a septum between the north and south pipes. **b** Photograph of the Venetia
941 K2 mine (looking northwest) showing the westward dipping shear surface which separates
942 the two halves of the pipe (K2 east and K2 west). Marked lithological contrasts occur
943 across the shear zone with massive volcaniclastic kimberlite (MVK) in contact with matrix-
944 supported volcaniclastic kimberlite breccias (mVKBr) on the lower bench, and with clast-
945 supported volcaniclastic kimberlite breccias (cVKBr) on upper bench. The sampling sites
946 which are within the field of view are numbered. **c** Photograph of the Venetia K1 mine
947 (looking northwest). K1 is predominately filled with MVK and the wall rock comprises
948 Proterozoic basement gneisses
949
950 Figure 3. Representative thermal demagnetization vector plots for basalt clasts from Orapa
951 A/K1. Solid squares represent the magnetization vector for each sample (projected on to the
952 horizontal plane) at different laboratory temperatures (in °C); open circles represent the
953 vector projected onto a vertical plane at the same laboratory temperature. **a, b** Type-1 two-
954 component magnetizations. **c, d** Two-component and single-component magnetization
955 obtained from exterior and interior of the same lithic clast. **e, f** Type-2 single component
956 magnetizations. **g, h** Type-3 (restricted T_{ub} spectra) single component magnetizations.
957
958 Figure 4. Equal area stereographic projections of palaeomagnetic directions recorded at
959 each sampling site at Orapa A/K1. Open symbols denote upper hemisphere projections;
960 solid symbols denote lower hemisphere projections. Small circle is the mean direction of
961 the data and the larger circle around the mean shows the 95% confidence limit of the mean
962 (expressed as an angular radius). Open star is the Cretaceous reference palaeomagnetic

direction (D = 350°, I = -69). **a** Low-temperature components in type-1 clasts from Site 5 (pyroclastic flow deposit). **b** High-temperature components in type-1 clasts from Site 5. **c** Type-2 single component magnetizations from NPK clasts (Sites 1 and 2). **d** Single-component magnetizations from Site 3 (Talus deposit). **e** Low-temperature and single components from Site 4 (Debris flow deposit).

Figure 5. Representative thermal demagnetization vector plots for lithic clasts from Venetia K1 and K2 pipes. Solid squares represent the magnetization vector for each sample (projected on to the horizontal plane) at different laboratory temperatures (in °C); open circles represent the vector projected onto a vertical plane at the same laboratory temperature. **a,b** Type-1 two-component magnetization. **c** Type-2 single component magnetization. **d, e** Type-3 (restricted T_{ub} spectra) single component magnetizations. **f, g, h** Type-4 (restricted T_{ub} spectra) single component magnetizations.

Figure 6. Equal area stereographic projections of palaeomagnetic directions recorded at each sampling site at Venetia K1 and K2. Open symbols denote upper hemisphere projections; solid symbols denote lower hemisphere projections. Small circle is the mean direction of data and the large circle around the mean shows the 95% confidence limit of the mean (expressed as an angular radius). Solid star is the Cambrian reference palaeomagnetic direction (D = 317.1°, I = 42.5°). Open star is the Cretaceous reference palaeomagnetic reference direction (D = 350°, I = - 69°). **a** Mesozoic overprint directions in Venetia K1 and K2 samples. **b** Cambrian overprint directions observed in 4 samples from Venetia K1 and K2.

Figure 7. Typical magnetic susceptibility-temperature curves for samples from **a, b** Orapa A/K1 SVK (Site 4), **c, d, f** Orapa A/K1 SVK (Site 5), **h, i** Orapa A/K1 NPK (Site 2), **j, k** Orapa A/K1 SVK (Site 3), **l, m** Venetia K2. **e, g, n** Representative thermal demagnetization plots for samples providing T_e estimates. The Curie temperatures (T_c) were determined using the inverse-susceptibility method of Petrovský and Kapička (2006).

Figure 8. SEM micrographs of Fe-Ti oxides within basalt and amphibolite samples. **a** Host titanomagnetite grain in basalt sample AK1-51a (T_e = 360-400°C); Ilmenite lamellae (dark grey) are observed along {111} cystallographic axes of the host titanomagnetite (light grey). **b** Host titanomagnetite grain in basalt sample AK1-76b2 (T_e ≥660°C). **c, d** Higher magnification view of Ti-poor titanomagnetite intergrowths in AK1-51a and AK-76b2 respectively. **e, f** Country rock basalt samples. **g** Ilmenite grain in amphibolite gneiss sample V60a (T_e ≥590°C) showing ilmenite, rutile and titanite intergrowths. The mottled regions are fine-grained intergrowths of Ti-poor titanomagnetite, rutile and illmenite. **h** Ilmenite grain in country rock amphibolites sample. *ilm* ilmenite, *rut* rutile, *ti* titanite, *tm* titanomagnetite.

Figure 9. T_e estimates obtained from individual lithic clasts. **a** Minimum T_e estimates obtained from Orapa A/K1 NPK lithic clasts provided by the maximum T_c of the minerals in the samples. The range of maximum T_c values and the number of individual samples displaying these values are shown. **b** T_e for individual samples in Orapa south pipe deposits. Downward pointing arrows indicate the data point is a maximum T_e estimate.

Upward pointing arrows indicate the data point is a minimum T_e estimate. Error bars indicate the upper and lower limits of each T_e estimate obtained from clasts displaying a two-component magnetization. Open symbols are used to indicate where different T_e estimates have been obtained from a single clast.

Figure 10. Schematic illustration of the different T_{dep} estimates for the various deposits in the Orapa and Venetia kimberlite pipes. Vent-filling pyroclastic breccias provide minimum T_{dep} values of >570°C. Deposits interpreted as ignimbrites have intermediate T_{dep} values and epiclastic deposits (debris flows and talus breccias) have been emplaced at ambient temperatures (<180°C). Estimates of the source temperature of the pyroclastic deposits are ~760–920°C.

Table 1: Statistics of magnetization components from lithic clasts from the Orapa A/K1and the Venetia K1 and K2 kimberlite pipes.

N, number of magnetization vectors; n, total number of samples studied; **N**/n is the number of stable magnetization vectors identified per number of studied samples; Dec., declination of the mean direction of magnetization of N vectors; Inc., inclination of the mean direction of magnetization of N vectors; R, vector resultant of N vectors; k best estimate of precision parameter; α_{95}, 95% confident limit; R_0 Watson's (1956) parameter; grouping is random for N vectors if $R<R_o$; asterisk*, too few data are available to calculate accurate statistical parameters (N<4)

Table 1

Orapa A/K1	Low-T_b component								High-T_b component							
Group or site	**N**/n	Dec.	Inc.	R	k	α_{95}	R_0	Ran.	N	Dec.	Inc.	R	k	α_{95}	R_0	Ran.
Site 1	**4**/4	11.7	-64	3.87	23.99	19.1	3.10	no								
Site 2	**51**/51	22	-64.5	48.67	21.49	4.4	11.53	no								
NPK	**55**/55	22.1	-64.5	52.54	21.93	4.2	11.97	no								
Site 3	**5**/5	83.6	-70.8	2.73	1.77	85.6	3.50	yes								
Site 4	**8**/8	3.7	-40.5	3.39	1.52	74.2	4.48	yes	1	213.6	-43.7		1.34		*	*
Site 5 (type-1)	**23**/23	330	-43.9	19.9	7.09	12.2	7.74	no	23	338.7	-66	11.86	1.97	30.4	7.74	no
Site 5 (type-2)	**5**/5	16.3	-37.6	1.47	1.13	>90	3.50	yes								
Site 5 (type-3)	**14**/14	201.9	60.6	3.58	1.25	75.7	5.98	yes								
Venetia	Low-T_b component								High-T_b component							
Group or site	**N**/n	Dec.	Inc.	R	k	α_{95}	R_0	Ran.	N	Dec.	Inc.	R	k	α_{95}	R_0	Ran.
K2 site 1	**12**/14	330.8	-49.7	7.87	2.7	33.3	5.52	no	3	299	0.5	1.42	1.3	>90	*	*
K2 site 2	**2**/2	356.5	-57.2	1.76	4.2	>90	*	*								
K2 site 3	**2**/4	4.9	-78.6	1.99	70.9	30.1	*	*	1	81	-55.4				*	*
K2 site 4	**1**/1	294.8	-38.8				*	*	1	338.8	25.7				*	*
K2 site 5	**1**/1	311.8	25.1				*	*								
K2 site 8	**2**/2	334.9	-16.4	1.3	1.4	>90	*	*	2	11.5	-58	0.9	0.9	>90	*	*
K2 site 9	**2**/4	223.2	-57.9	1.37	1.6	>90	*	*	1	8.3	-7.6				*	*
K2 site10	**0**/5															
K1 (site 1)	**2**/2	301.1	-74.1	1.7	3.4	>90	*	*	1	350.5	-21.6				*	*
Cambrian	**4**	308.2	46.2	3.13	3.4	58.5	3.10	no								
Mesozoic	**20**	329.8	-64.4	16.69	5.7	14.9	7.17	no								
All clasts	**24**/35	324.8	-54.1	15.79	2.8	21.9	7.91	no	9	347	-21.9	4.41	1.7	58.2	4.76	Yes

Figure 1

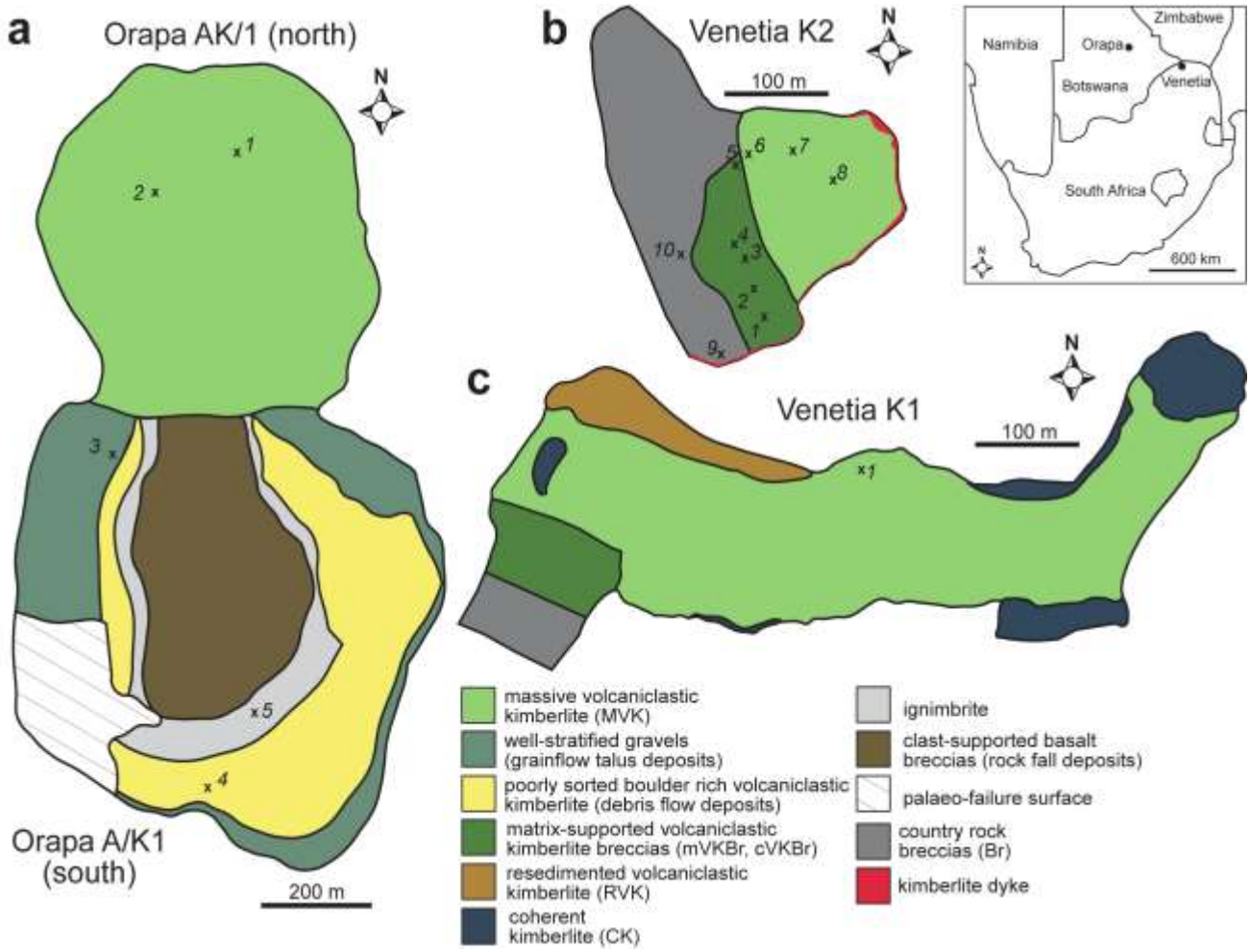
a
Orapa AK/1 (north)
N
1
2
3
4
5
Orapa A/K1
(south)
200 m
b
Venetia K2
N
100 m
1
2
3
4
5
6
7
8
9
10
Namibia
Zimbabwe
Orapa
Botswana
Venetia
South Africa
N
600 km
c
Venetia K1
N
100 m
1
massive volcaniclastic kimberlite (MVK)
well-stratified gravels (grainflow talus deposits)
poorly sorted boulder rich volcaniclastic kimberlite (debris flow deposits)
matrix-supported volcaniclastic kimberlite breccias (mVKBr, cVKBr)
resedimented volcaniclastic kimberlite (RVK)
coherent kimberlite (CK)
ignimbrite
clast-supported basalt breccias (rock fall deposits)
palaeo-failure surface
country rock breccias (Br)
kimberlite dyke

Figure 2

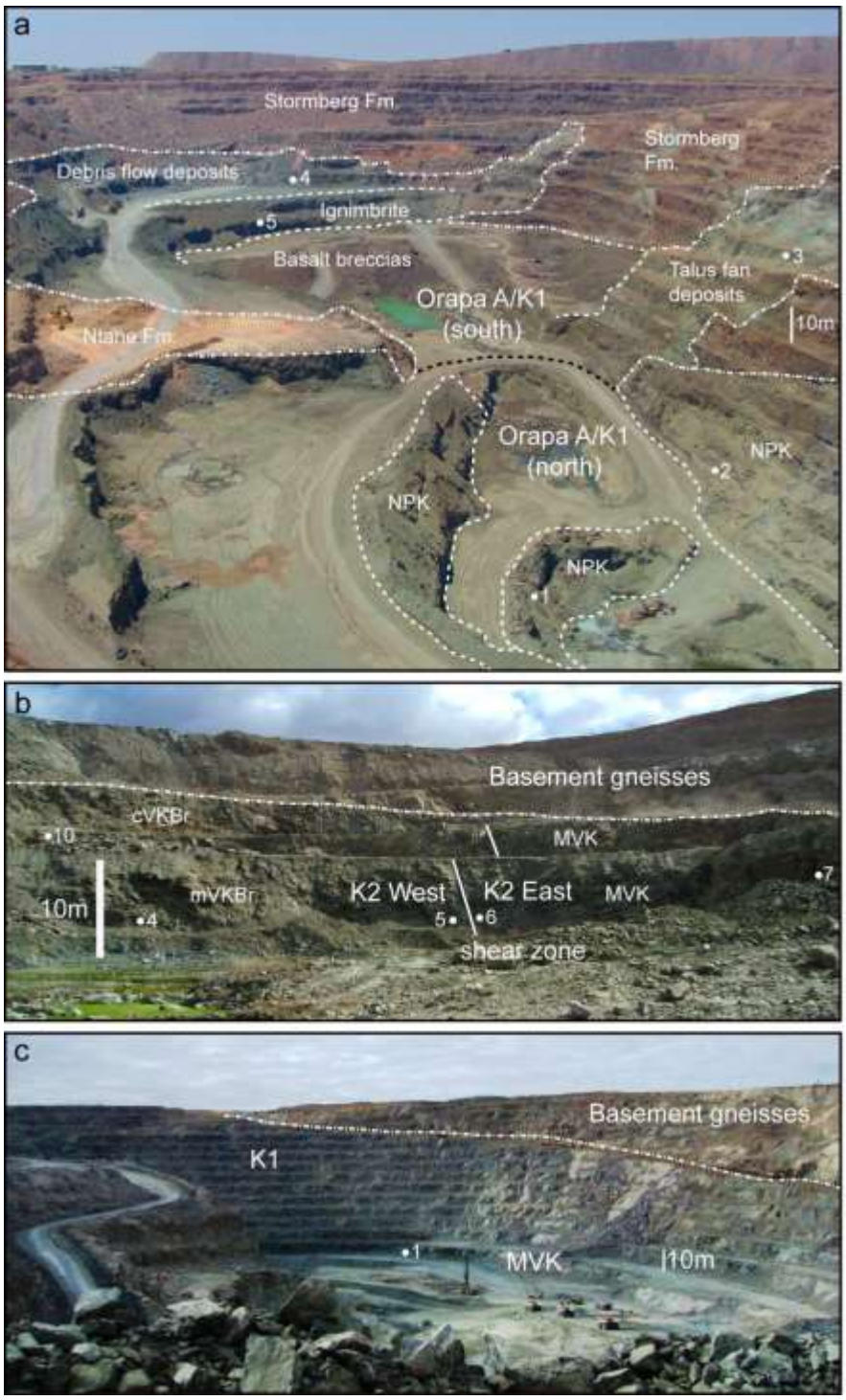
a
Stormberg Fm
Stormberg Fm
Debris flow deposits
•4
Ignimbrite
•5
Basalt breccias
Talus fan deposits
•3
Orapa A/K1 (south)
10m
Ntane Fm
Orapa A/K1 (north)
NPK
•2
NPK
NPK
•1
b
Basement gneisses
cVKBr
•10
MVK
•7
10m
mVKBr
•4
K2 West
K2 East
MVK
5•
•6
shear zone
c
Basement gneisses
K1
•1
MVK
10m

Figure 3

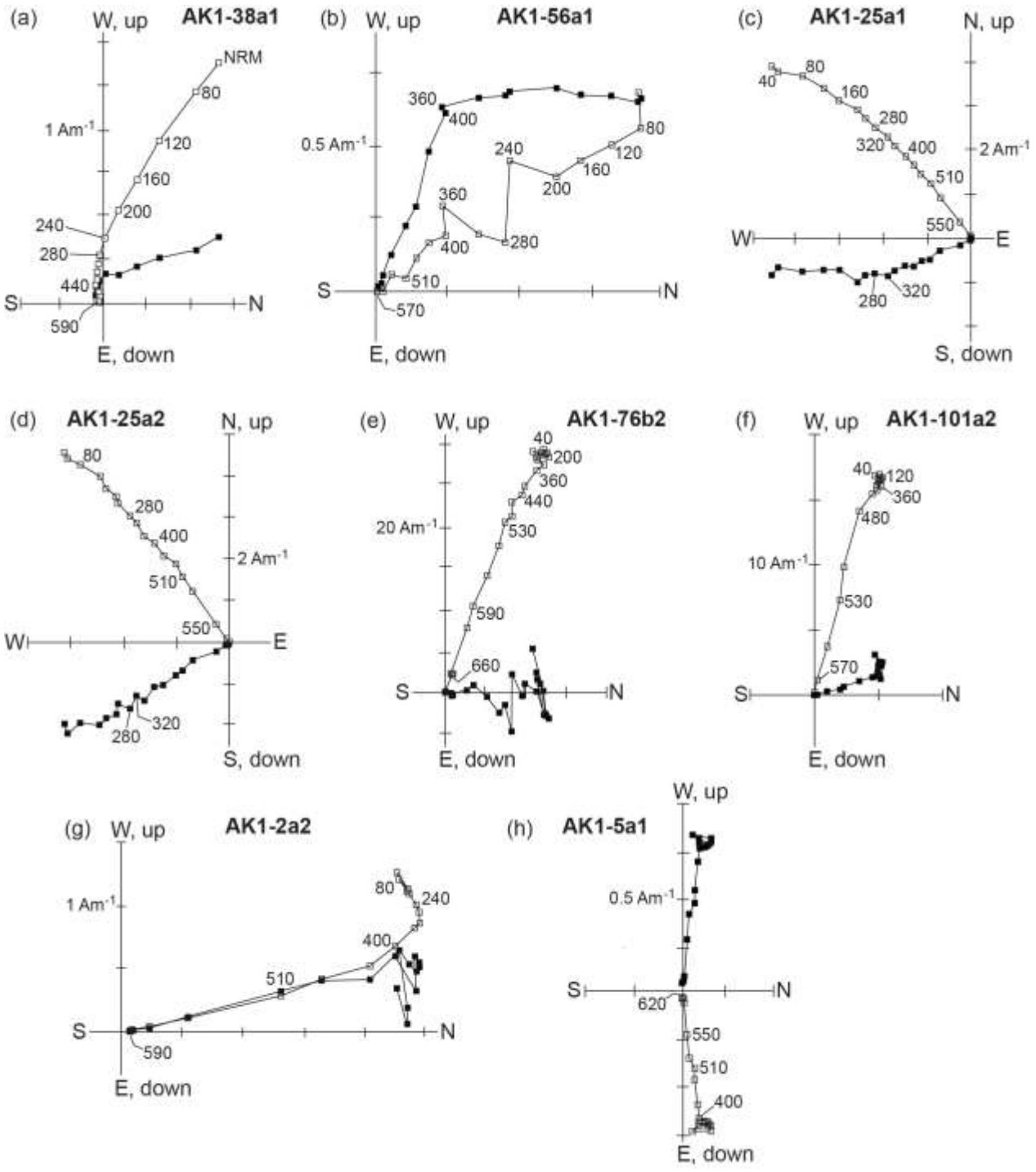
(a)
W, up
AK1-38a1
NRM
80
1 Am-1
120
160
200
240
280
440
S
N
590
E, down
(b)
W, up
AK1-56a1
360
400
80
0.5 Am-1
240
120
160
200
360
280
400
S
510
N
570
E, down
(c)
AK1-25a1
N, up
40
80
160
280
320
400
2 Am-1
510
550
W
E
280
320
S, down
(d)
AK1-25a2
N, up
80
280
400
2 Am-1
510
550
W
E
280
320
S, down
(e)
W, up
AK1-76b2
40
200
360
440
20 Am-1
530
590
660
S
N
E, down
(f)
W, up
AK1-101a2
40
120
360
480
10 Am-1
530
570
S
N
E, down
(g)
W, up
AK1-2a2
1 Am-1
80
240
400
510
S
N
590
E, down
(h)
W, up
AK1-5a1
0.5 Am-1
S
N
620
550
510
400
E, down

Figure 4

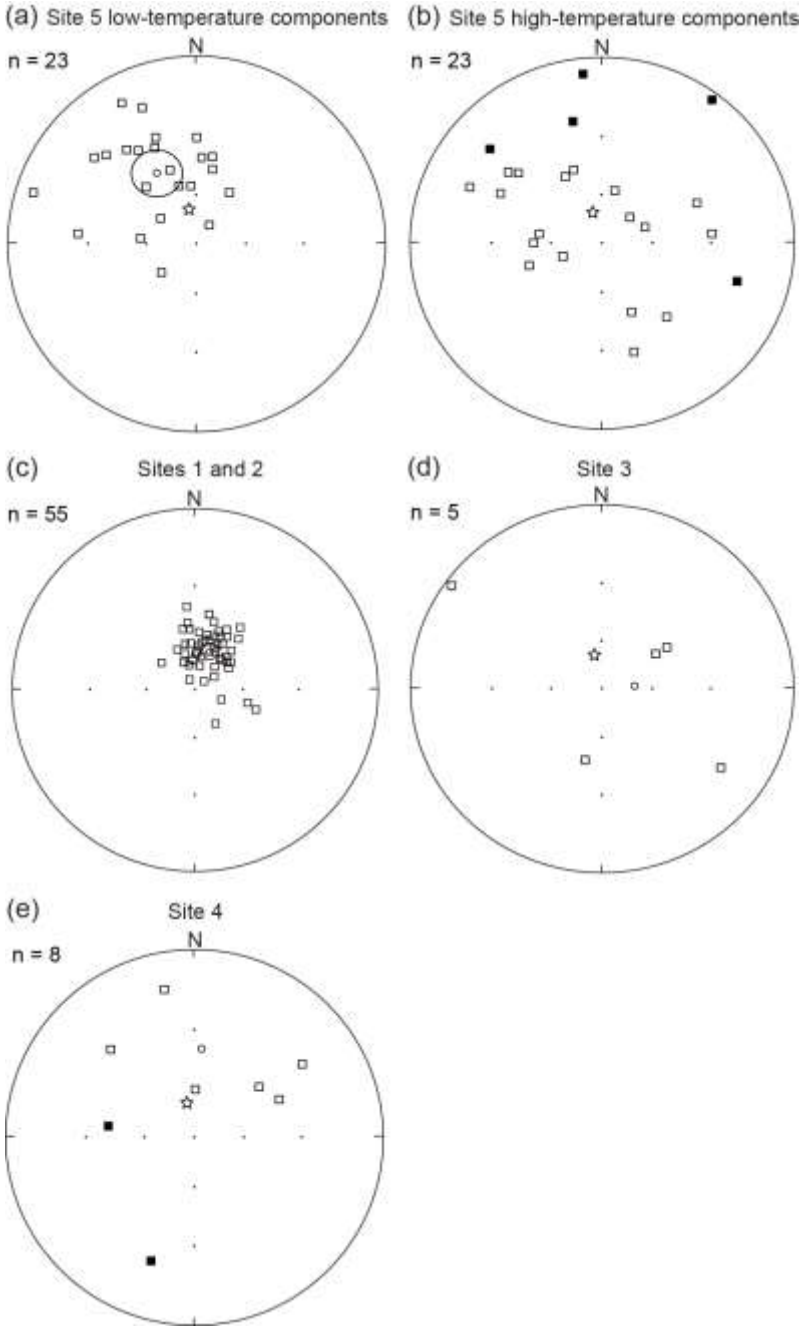
(a) Site 5 low-temperature components
n = 23
N
(b) Site 5 high-temperature components
n = 23
N
(c) Sites 1 and 2
n = 55
N
(d) Site 3
n = 5
N
(e) Site 4
n = 8
N

Figure 5

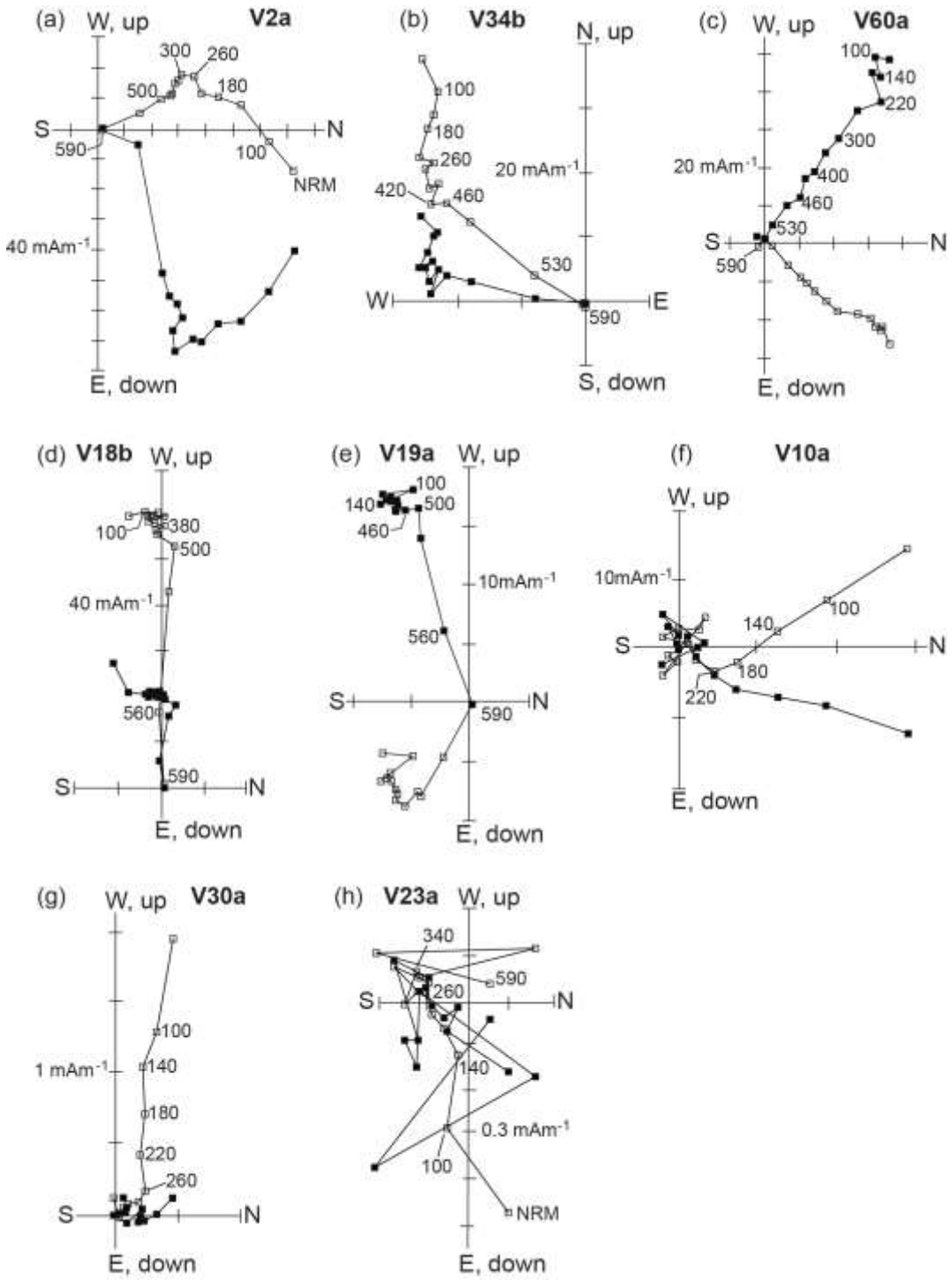
(a) W, up V2a
300
260
500
180
S
N
590
100
NRM
40 mAm-1
E, down
(b) V34b
N, up
100
180
260
20 mAm-1
420
460
530
W
E
590
S, down
(c) W, up V60a
100
140
220
300
20 mAm-1
400
460
530
S
N
590
E, down
(d) V18b W, up
100
380
500
40 mAm-1
560
S
590
N
E, down
(e) V19a W, up
100
140
500
460
10mAm-1
560
S
N
590
E, down
(f) V10a
W, up
10mAm-1
140
100
S
N
180
220
E, down
(g) W, up V30a
100
1 mAm-1
140
180
220
260
S
N
E, down
(h) V23a W, up
340
590
S
260
N
140
0.3 mAm-1
100
NRM
E, down

Figure 6

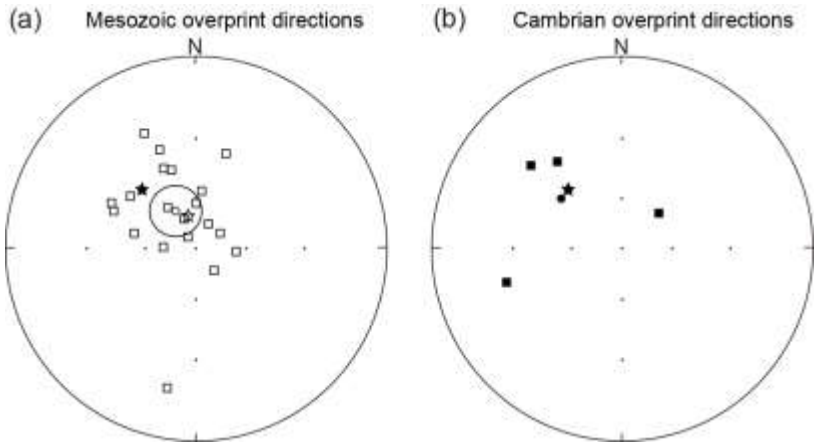
(a)
Mesozoic overprint directions
N
(b)
Cambrian overprint directions
N

Figure 7

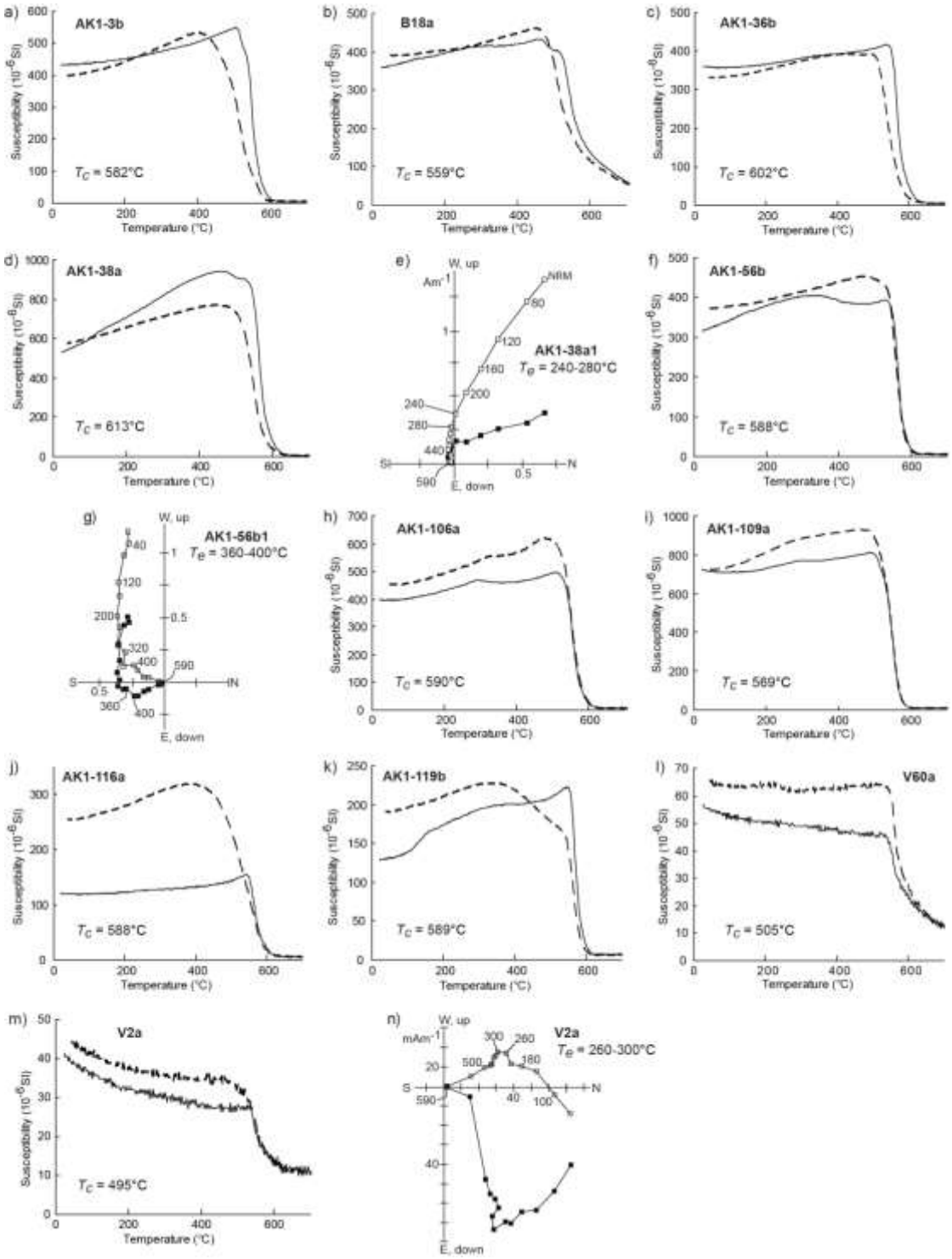
a)
AK1-3b
T_C = 582°C
b)
B18a
T_C = 559°C
c)
AK1-36b
T_C = 602°C
d)
AK1-38a
T_C = 613°C
e)
W, up
Am^{-1}
NRM
80
120
160
200
240
280
440
590
AK1-38a1
T_e = 240-280°C
S
N
E, down
f)
AK1-56b
T_C = 588°C
g)
W, up
AK1-56b1
T_e = 360-400°C
40
120
200
320
400
590
360
S
N
E, down
h)
AK1-106a
T_C = 590°C
i)
AK1-109a
T_C = 569°C
j)
AK1-116a
T_C = 588°C
k)
AK1-119b
T_C = 589°C
l)
V60a
T_C = 505°C
m)
V2a
T_C = 495°C
n)
W, up
mAm^{-1}
300
260
180
100
500
590
40
V2a
T_e = 260-300°C
S
N
E, down
Susceptibility (10^{-6}SI)
Temperature (°C)

Figure 8

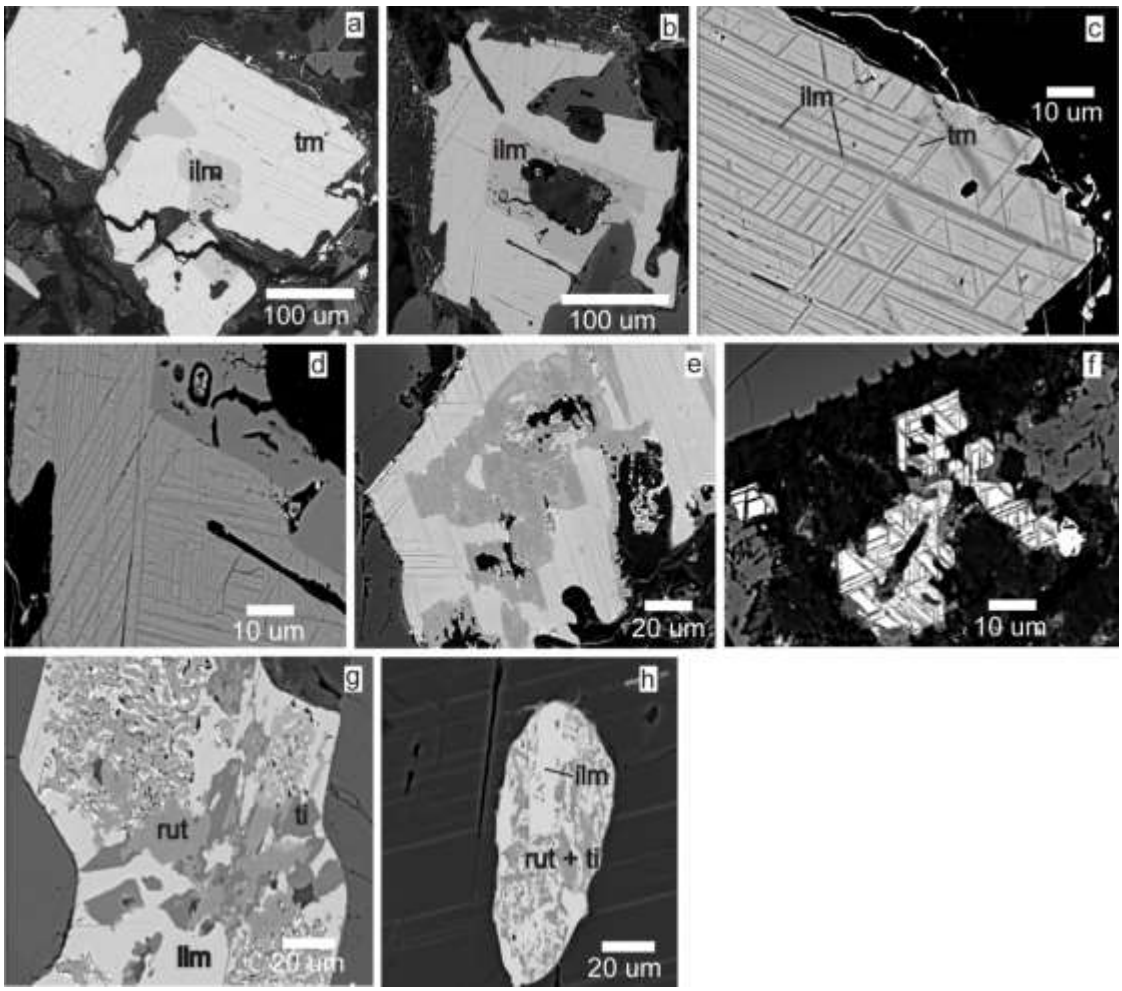
a
tm
ilm
100 um
b
ilm
100 um
c
ilm
tm
10 um
d
?
10 um
e
20 um
f
10 um
g
rut
ti
ilm
20 um
h
ilm
rut + ti
20 um

Figure 9

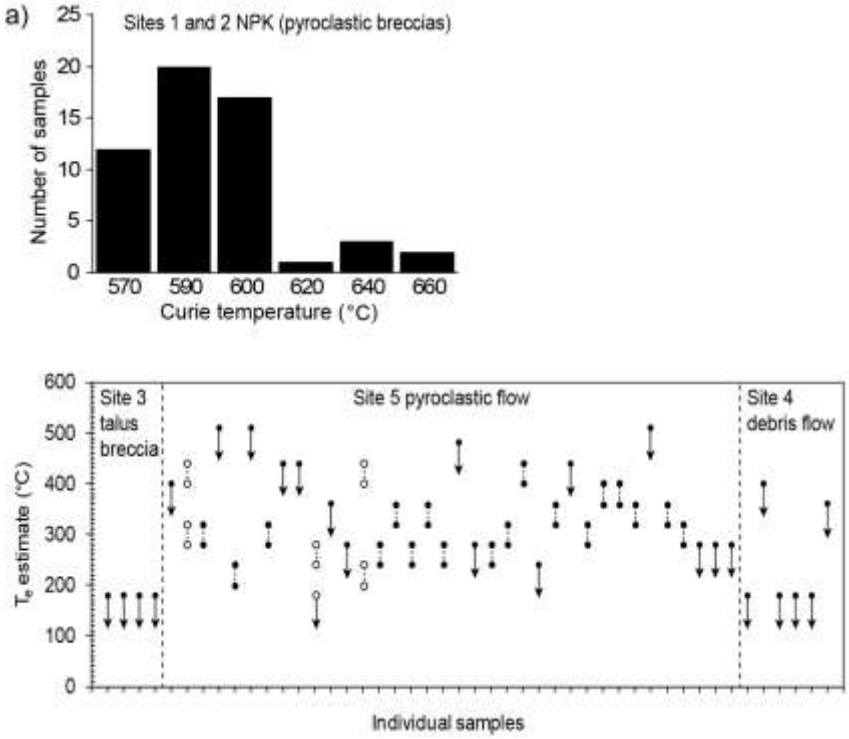
a)
Sites 1 and 2 NPK (pyroclastic breccias)
Number of samples
25
20
15
10
5
0
570
590
600
620
640
660
Curie temperature (°C)
Site 3
talus
breccia
Site 5 pyroclastic flow
Site 4
debris flow
T_e estimate (°C)
600
500
400
300
200
100
0
Individual samples

Figure 10

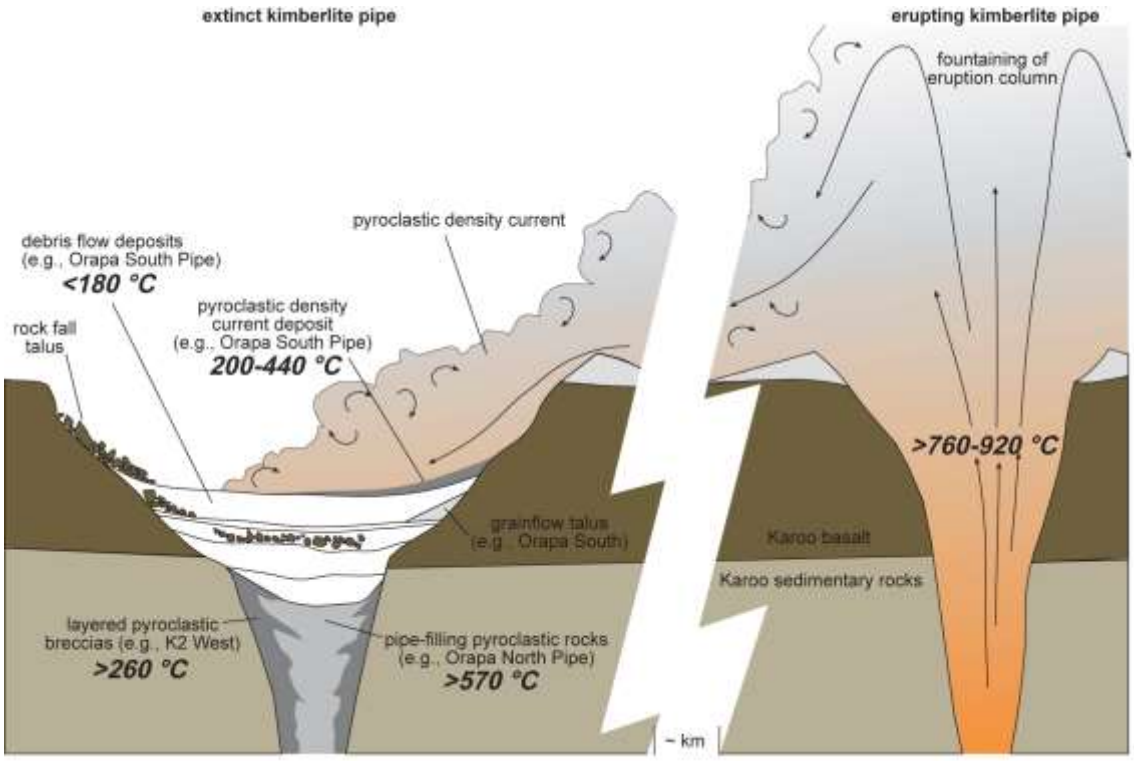
extinct kimberlite pipe
erupting kimberlite pipe
fountaining of eruption column
pyroclastic density current
debris flow deposits (e.g., Orapa South Pipe)
<180 °C
pyroclastic density current deposit (e.g., Orapa South Pipe)
200-440 °C
rock fall talus
>760-920 °C
grainflow talus (e.g. Orapa South)
Karoo basalt
Karoo sedimentary rocks
layered pyroclastic breccias (e.g., K2 West)
>260 °C
pipe-filling pyroclastic rocks (e.g., Orapa North Pipe)
>570 °C
~ km